© 2020. Published by The Company of Biologists Ltd | Journal of Experimental Biology (2020) 223, jeb216945. doi:10.1242/jeb.216945

RESEARCH ARTICLE

# *nkx3.2* mutant zebrafish accommodate jaw joint loss through a phenocopy of the head shapes of Paleozoic jawless fish

**Tetsuto Miyashita[1,2,*], Pranidhi Baddam[3], Joanna Smeeton[4], A. Phil Oel[2,5], Natasha Natarajan[4], Brogan Gordon[2], A. Richard Palmer[2], J. Gage Crump[4], Daniel Graf[3,6] and W. Ted Allison[2,6,‡]**

## ABSTRACT

The vertebrate jaw is a versatile feeding apparatus. To function, it requires a joint between the upper and lower jaws, so jaw joint defects are often highly disruptive and difficult to study. To describe the consequences of jaw joint dysfunction, we engineered two independent null alleles of a single jaw joint marker gene, *nkx3.2*, in zebrafish. These mutations caused zebrafish to become functionally jawless via fusion of the upper and lower jaw cartilages (ankylosis). Despite lacking jaw joints, *nkx3.2* mutants survived to adulthood and accommodated this defect by: (a) having a remodeled skull with a fixed open gape, reduced snout and enlarged branchial region; and (b) performing ram feeding in the absence of jaw-generated suction. The late onset and broad extent of phenotypic changes in the mutants suggest that modifications to the skull are induced by functional agnathia, secondarily to *nkx3.2* loss of function. Interestingly, *nkx3.2* mutants superficially resemble ancient jawless vertebrates (anaspids and furcacaudiid thelodonts) in overall head shape. Because no homology exists in individual skull elements between these taxa, the adult *nkx3.2* phenotype is not a reversal but rather a convergence due to similar functional requirements of feeding without moveable jaws. This remarkable analogy strongly suggests that jaw movements themselves dramatically influence the development of jawed vertebrate skulls. Thus, these mutants provide a unique model with which to: (a) investigate adaptive responses to perturbation in skeletal development; (b) re-evaluate evolutionarily inspired interpretations of phenocopies generated by gene knockdowns and knockouts; and (c) gain insight into feeding mechanics of the extinct agnathans.

**KEY WORDS: Skeletal remodeling, Developmental plasticity, Skull, Ankylosis, Gnathostome, Agnatha, CRISPR, TALEN, *bapx***

## INTRODUCTION

The jaw is a functionally versatile innovation that facilitated explosive diversification of gnathostomes (a clade containing jawed vertebrates), but its basic structure is surprisingly simple and highly conserved (Miyashita, 2016). A jaw consists of 'a hinge and caps': upper and lower skeletal levers hinged at a jaw joint (Depew and Simpson, 2006). As the joint enables biting motions, its origin is considered the critical step in the evolutionary assembly of the vertebrate jaw (Cerny et al., 2010; Kuratani, 2012; Miyashita, 2016). Across jawed vertebrates, the presumptive jaw joint is marked by the expression of *nkx3.2*, an NK2 class homeobox gene (a.k.a. *bapx*), at the mid-height of the embryonic mandibular arch (Gillis et al., 2013; Lukas and Olsson, 2018a; Miller et al., 2003; Tucker et al., 2004). Chondrogenesis dorsal to this expression domain gives rise to a palatoquadrate (upper jaw), whereas chondrogenesis ventral to it forms Meckel's cartilage (lower jaw) (Medeiros and Crump, 2012). This basic pattern remains conserved among jawed vertebrates, but later development varies. Marginal bones arise intramembranously around the often endo-/peri-chondrally ossified jaw cartilages, except in chondrichthyans (sharks, rays and skates) (Hall, 2015). In mammals, the jaw joint forms between two such intramembranous bones (temporal and dentary), whereas the proximal jaw joint becomes the malleus–incus interface that is, in mice, no longer affected by *Nkx3.2* knockout (Tucker et al., 2004). Despite these variations after pharyngeal chondrogenesis, no gnathostome lineage has secondarily lost functional jaws.

Our aim here was to find out whether – and how – jaw function affects vertebrate skull shape during development. Clinically documented agnathia in humans typically accompanies severe congenital disorders such as holoprosencephaly (forebrain defect with a failure to form cerebral hemispheres) and otocephaly (lethal malformation of the first pharyngeal arch), but jaw loss is clearly a secondary effect and not a cause in these cases (Bixler et al., 1985; Brown and Marsh, 1990; Gekas et al., 2010; Schiffer et al., 2002). Instances of temporomandibular joint ankylosis (stiffening of the mammalian jaw joint due to bone fusion) may result from trauma or infection, or may be congenital (Adekeye, 1983; Chidzonga, 1999; Manganello-Souza and Mariani, 2003). If untreated, the ankylosis can lead to the 'bird face' deformity in humans (El-Sheikh et al., 1996). However, these cases do not fully document the effects of functional jaw loss. In mammalian models, various jaw/skull deformations have been induced by surgical resection, detachment or repositioning of the jaw muscles and/or bones (Bayram et al., 2010; Gomes et al., 2012; Horowitz and Shapiro, 1955; Lifshitz, 1976; Miyazaki et al., 2016; Rodrigues et al., 2009; Sarnat, 1970; Sarnat and Muchnic, 1971; Toledo et al., 2014). These manipulations occurred well after formation of the jaw skeleton and muscles, and the jaws remained partially functional because operations were unilateral or because surgeries only affected a component of the jaw system. The defects and deformities reported in these studies imply: (a) jaw movements are potentially an important factor in shaping the skull; and (b) any allele disrupting jaw movements would be generally maladaptive. Nevertheless,

[1]Department of Organismal Biology and Anatomy, University of Chicago, Chicago, IL 60637, USA. [2]Department of Biological Sciences, University of Alberta, Edmonton, AB, Canada T6G 2E9. [3]Department of Dentistry, University of Alberta, Edmonton, AB, Canada T6G 2R3. [4]Department of Stem Cell Biology and Regenerative Medicine, W. M. Keck School of Medicine, University of Southern California, Los Angeles, CA 90033, USA. [5]Developmental Biology Unit, European Molecular Biology Laboratory, 69117 Heidelberg, Germany. [6]Department of Medical Genetics, University of Alberta, Edmonton, AB, Canada T6G 2R7.
*Present address: Canadian Museum of Nature, PO Box 3443, Station D, Ottawa, ON, Canada K1P 6P4.

‡Author for correspondence (ted.allison@ualberta.ca)

T.M., 0000-0003-0050-4594; A.R.P., 0000-0002-7579-3899; W.T.A., 0000-0002-8461-4864

**Received 18 October 2019; Accepted 1 June 2020**

these implications from mammalian systems are difficult to explore without an accessible experimental model.

To fill this gap, we engineered two distinct null alleles of *nkx3.2* in zebrafish. Previously, transient knockdown of *nkx3.2* during early development (using morpholinos) resulted in fusion of the nascent jaw cartilages in both zebrafish and frogs (Lukas and Olsson, 2018a; Miller et al., 2003). We confirmed in zebrafish that the mutants recapitulate this phenotype. Surprisingly, mutant zebrafish are viable – despite loss of the jaw joints – and grow through to adulthood. Functionally jawless as a result, *nkx3.2*$^{-/-}$ zebrafish develop dramatically altered skull shape: the mouth is fixed open, the snout reduced and the branchial region expanded. The late onset and broad extent of morphological changes indicate that this open-mouth phenotype is induced by functional agnathia, secondarily to *nkx3.2* loss of function. Although previously unknown in zebrafish or any other jawed vertebrates, similar head shapes also occurred in two extinct lineages of ≥400 million year old jawless vertebrates, anaspids and thelodonts. In the absence of any homology in individual facial bones, this convergence implies that the adult mutant phenotype is an adaptive response to functional requirements of feeding without mobile jaws. Thus, *nkx3.2* mutant zebrafish provide a unique model for both skeletal remodeling and joint diseases, and to re-evaluate evolutionary implications of mutant phenocopies in general.

## MATERIALS AND METHODS

### Animal ethics

Zebrafish [*Danio rerio* (F. Hamilton 1822)] maintenance and experiments were approved as protocol number AUP00000077 by the Animal Care and Use Committee: Biosciences at the University of Alberta, as dictated by the Canadian Council on Animal Care. Other zebrafish work was approved by the University of Southern California Institutional Animal Care and Use Committee.

### Animal husbandry

Embryos were incubated at 28°C, and treated with 0.003% PTU (1-phenyl-2-thiourea) in 10% Hank's saline starting at 24 h post-fertilization (hpf). Larvae were introduced into the nursery at 1 week to 10 days post-fertilization (dpf). Genomic DNA was extracted from clipped fins of 3–5 dpf larvae or from adults.

### Molecular genetics

Nkx3.2 protein is a transcription factor with a homeobox DNA binding domain that is 100% conserved in amino acid sequence among zebrafish, mouse and human homologs. In zebrafish, a single *nkx3.2* gene is apparent in the genome, and its homology to mammalian *NKX3.2* is strongly supported by gene synteny, e.g. the neighbor genes flanking *nkx3.2* on zebrafish Chromosome 14 (*wdr1* and *bod1l1*) are positioned coordinately in mouse, human and spotted gar.

Two disparate regions of the gene were targeted by CRISPR or TALEN, producing two disparate null alleles that produced similar phenotypes (Fig. 1A). One allele, *nkx3.2*$^{ua5011}$, was engineered with CRISPR/Cas9 (Gagnon et al., 2014) targeted at the beginning of the homeodomain, and harbors a 20 bp deletion resulting in a frameshift (Fig. 1A; Dryad data supplement 1, https://doi.org/10.5061/dryad.8w9ghx3j9). The disrupted translation of codons is predicted to abrogate production of the critical homeobox domain, and instead produce random amino acids. This is predicted to produce a non-functional Nkx3.2 protein and a null allele. A disparate allele (el802) was generated using TALEN (Barske et al., 2016) targeted at the start of the gene. This produced a stably inherited gene with 14 bp deletion, removing A of the ATG translation start codon (Fig. 1A). The allele *nkx3.2*$^{el802}$ is predicted to not produce Nkx3.2 protein. Morphologically, these two alleles are not readily distinguishable from each other (see Results).

### CRISPR

To generate *nkx3.2*$^{ua5011}$, we designed sgRNA to five different targets near or within the *nkx3.2* homeodomain, which were all injected: GGCGGCCATCTGACGTCGCT; GGCTGACGCCAG-CAGATCGG; AAGCAGCGGAAGAAGCGCTC; GAGCGCTT-CTTCCGCTGCTT; and GGCCGCGTTCTCCCACGCGC. These targets were selected using the web resource CHOPCHOP (Labun et al., 2016; Montague et al., 2014). Following the protocol developed by Gagnon and colleagues (2014), we prepared a template for each sgRNA using two different oligonucleotides: one containing a target sequence led by the SP6 promoter (ATTTAGGTGACACTATA) and followed by the overlapping region (GTTTTAGAGCTAGAAATAGCAAG) of the reverse oligonucleotide, and the reverse containing the constant, Cas9-binding domain of sgRNA. These oligonucleotides were annealed after 5 min incubation at 95°C, through graded cooling (−2°C s$^{-1}$ to 85°C; −0.1°C s$^{-1}$ to 25°C), and filled in for the non-overlapping regions using T4 DNA polymerase (NEB: M0203S). To synthesize sgRNAs using these templates, MegaScriptTM SP6 Transcription Kit (Ambion: AM1330) was used. The RNAs were precipitated in ammonium acetate solution, resuspended in UltraPure™ $H_2O$ and stored in 2–3 µl aliquots at −80°C. For injection, sgRNAs were diluted to 400–600 ng µl$^{-1}$, and 1 µl was mixed with 1 µl aliquot of Cas9 nuclease from *Streptococcus pyogenes* (NEB: M0646) at 1 µg ml$^{-1}$. This solution was mixed with 3 µl of 0.2 mol l$^{-1}$ KCl, 0.2% Phenol Red and dd$H_2O$. The final injection volume per embryo was approximately 5 nl, containing 400–600 pg sgRNA and 1 ng Cas9 nuclease. For control, GFP 5′GA was used in $P_0$ (ubi:switch/RH+AB was crossed at this stage), which can be phenotyped by reduction of ubiquitous GFP in the progenies with dsRed expression in the heart.

We generated *nkx3.2*$^{ua5011}$ against an AB background. Cas 9 and sgRNAs targeted for *nkx3.2* were co-injected with sgRNA that disrupts GFP GA5′ (CTCGGGCTGAAGCTCGGCG), at stages between fertilization and first cleavage, into fertilized eggs collected from the crossing of ua3140 ubi:switch/AB+RH and the background AB line. At 3 dpf, injected larvae were sorted for reduced expression of ubiquitous GFP and the presence of dsRed fluorescence in the heart. These larvae provided the $P_0$ population. Sequencing of genomic DNA extracted from fin clips of the $P_0$ adults identified a female with a 20 bp deletion in the homeodomain-coding region of *nkx3.2* (ua5011). The $P_0$ female carrying this mutation was crossed to the *sox10*:GFP transgenic line, and progenies were sorted at 3 dpf for the presence of *sox10*:GFP expression and the absence of the two markers (ubiquitous GFP expression and fluorescent red heart). ua5011 heterozygotes were identified by both sequencing of extracted gDNA and restriction fragment length polymorphism (RFLP) analysis using one XmaI (NEB: R01805) restriction site within the deleted region (primers for genotyping: 5′-GGACGAGACGGATCAGGAATC-3′; 5′-CACTCGGCGTGTTCGGTAAA-3′). These $F_1$ heterozygotes were incrossed for $F_2$ embryos, which were genotyped by RFLP analysis and phenotyped at 4 dpf by identifying *sox10*:GFP-positive chondrocytes and staining cartilages using Alcian Blue. Homozygotes were reared with a strictly small-grained diet to the adult stage. In this study, *nkx3.2*$^{ua5011}$ fish represent the $F_2$ generation

Journal of Experimental Biology (2020) 223, jeb216945. doi:10.1242/jeb.216945

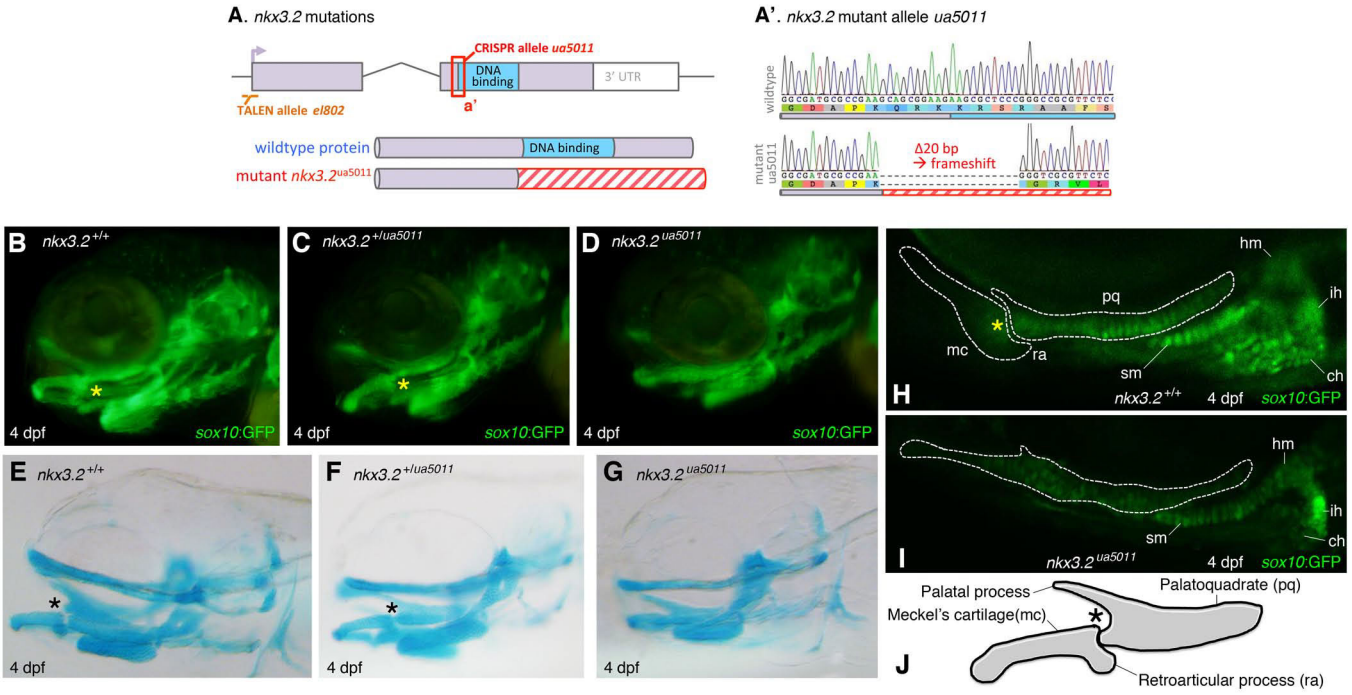


**Fig. 1. Null alleles of *nkx3.2* in zebrafish result in jaw joint ankylosis.** (A) Mutations in the zebrafish gene *nkx3.2* that encodes the homeobox transcription factor protein Nkx3.2 (aka Bapx1). (A) Left: the *nkx3.2* gene contains two exons (purple), the second of which encodes the homeobox domain (DNA binding domain, blue). The diagram is approximately to scale (exon 1=310 bp), except the 3′ untranslated region (3′UTR). Allele *nkx3.2*$^{el802}$ was generated with TALEN technology that deleted 14 bp from the start of the gene (orange dashed line), including A of the ATG start codon. Allele *nkx3.2*$^{ua5011}$ was engineered with CRISPR/Cas9 to generate a 20 bp deletion (red box) and frameshift that is predicted to eliminate the homeodomain. Below is a schematic diagram of the predicted protein following CRISPR mutagenesis. In the allele *nkx3.2*$^{ua5011}$, the frameshift (20 bp deletion) is predicted to disrupt the translation and abrogate production of the critical homeobox domain. This is predicted to produce random amino acids (red hatching). Left: sequence from allele *nkx3.2*$^{ua5011}$ compared with wild-type. (B–I) At 4 days post-fertilization (dpf), the chondrocrania are compared by *sox10*:eGFP expression in chondrocytes (B–D,H,I) or by Alcian Blue staining of cartilages (E–G) between age-matched specimens. (B,E) The chondrocranial morphology of wild-type zebrafish (AB strain; *sox10*:eGFP) at 4 dpf in left lateral view by *sox10*:eGFP expression (B) and Alcian Blue staining (E). (C,F) The chondrocranial morphology of *nkx3.2* heterozygous mutants (*nkx3.2*$^{+/ua5011}$; *sox10*:eGFP) at 4 dpf in left lateral view by *sox10*:eGFP expression (C) and Alcian Blue staining (F). (D,G) The chondrocranial morphology of *nkx3.2* homozygous mutants (*nkx3.2*$^{ua5011}$; *sox10*:eGFP) at 4 dpf in left lateral view by *sox10*:eGFP expression (D) and Alcian Blue staining (G). (H,I) Comparison of jaw morphology between age-matched wild-type (AB; *sox10*:eGFP) (H) and *nkx3.2* homozygous mutants (*nkx3.2*$^{ua5011}$; *sox10*:eGFP) (I) at 4 dpf in left lateral view, using chondrocytes expressing *sox10*:eGFP. White dashed lines delineate the mandibular cartilages. (J) Schematic drawing of the mandibular cartilages in zebrafish at 4 dpf in left lateral view, showing wild-type morphology. In this and Figs 2, 3, 5–7, asterisks indicate the jaw joint. Abbreviations used: aa, anguloarticular; am, adductor mandibulae; ar, articular; bh, basihyal; cb, ceratobranchial; ch, ceratohyal; cl, cleithrum; co, coracoid; d, dentary; en, entopterygoid; ept, ectopterygoid; et, ethmoid; ex, exoccipital; f, frontal; hm, hyomandibula; ih, interhyal; io, interopercular; j, jugal; k, kinethmoid; le, lateral ethmoid; lp, lower lip; m, maxilla; mc, Meckel's cartilage; mpt, metapterygoid; n, nostril or aperture of nasohypophyseal system; na, nasal; o, operculum; or1, infraorbital 1; os, orbitosphenoid; pa, parietal; pcf, pectoral fin; pm, premaxilla; po, preopercular; pq, palatoquadrate; ps, parasphenodi; pt, pterygoid; pto, pterotic; pts, pterosphenoid; pvf, pelvic fin; q, quadrate; ra, retroarticular process; sm, symplectic; sn3, supraneural 3; so, subopercular; sp, sphenotic; sr, supraorbital; su, supraoccipital; tr, tripus; up, upper lip.

derived from the $P_0$ mutant female and a wild-type male (AB; *sox10*:GFP), whereas the comparative wild-type (AB; *sox10*:GFP) fish come from incrossing of half-siblings of the $P_0$ male.

### Tissue preparation and histology

One- and two-month-old *nkx3.2*$^{+/+}$ and *nkx3.2*$^{-/-}$ zebrafish were fixed in 4% paraformaldehyde (PFA) for 24 h. Zebrafish were eviscerated prior to decalcification with 0.5 mol $l^{-1}$ EDTA for 4 weeks. Samples were dehydrated post-decalcification in a series of graded ethanol and embedded in paraffin. Tissue blocks were embedded in a sagittal orientation and sections were cut at 7 µm using a 820 Spencer microtome. Hematoxylin and eosin staining was performed on zebrafish sections by firstly placing sections in an oven at 60°C for 10 min. The deparaffinized sections were rehydrated using xylene and graded ethanol (100%, 95%, 70%), followed by staining with hematoxylin and eosin. The slides were then dehydrated and mounted using Permount.

### Skeletal preparation

Alcian Blue staining of cartilages partly followed the protocol developed by Michael Shapiro (University of Utah). Specimens fixed in 4% PFA were rinsed with $ddH_2O$ and transferred to 70% ethanol. Once equilibrated, larvae were immersed in Alcian Blue solution (0.167 mg $ml^{-1}$ Alcian Blue, 15% acetic acid, 70% ethanol), rinsed through an ethanol/$ddH_2O$ series, and washed in a saturated sodium borate solution. Specimens were immersed in trypsin solution (0.125% trypsin, 30% sodium borate) overnight, washed in 1% KOH solution, bleached in 0.15% $H_2O_2$, 0.1% KOH, 25% glycerol solution, and immersed through a 1% KOH/glycerol graded series into 100% glycerol for storage. Specimens older than 21 dpf were immersed in 0.005% Alizarin Red solution in 1% KOH overnight, after the first 1% KOH wash and before bleaching in 0.15% $H_2O_2$, 0.1% KOH. We selected intact skeletal preparations for linear morphometrics (wild-type: 4 dpf, *n*=7; 14 dpf, *n*=7; 21 dpf, *n*=27; 30 dpf, *n*=60; 60 dpf, *n*=21;

*nkx3.2*$^{ua5011}$: 4 dpf, *n*=5; 14 dpf, *n*=9; 21 dpf, *n*=22; 30 dpf, *n*=42; 60 dpf, *n*=18).

## Filming

Wild-type (AB; *sox10*:GFP) and *nkx3.2*$^{ua5011}$ (one male and female for each genotype) were filmed at 2 months post-fertilization (mpf) to show feeding (Movie 1). A fish was placed in a 1.4 l tank with a dark background and given brine shrimp larvae. Feeding was filmed using Canon EOS 760D at 30 frames $s^{-1}$ in dimensions of 1280×720 pixels. The films were cropped and assembled using iMovie (v. 10.1.9, © 2001–2018 Apple Inc.) and slowed to 1/10 original speed.

## Imaging

### Micro-computed tomography (µCT)

Wild-type (AB; *sox10*:GFP) and *nkx3.2*$^{ua5011}$ zebrafish were scanned using MILabs µCT at the School of Dentistry, University of Alberta. For µCT scanning, 2-month-old individuals were selected from two different $F_2$ populations for each genotype (wild-type: *n*=10; *nkx3.2*$^{ua5011}$: *n*=11), fixed in 4% PFA for 24 h, and dehydrated in a graded ethanol series. The following parameters were applied for scanning: voxel size 10 µm, voltage 50 kV, current 0.24 mA and exposure time 75 ms. Skeletons were reconstructed by selecting and delineating regions of high tissue density at a voxel size of 25 µm using AVIZO (Milabs, Utrecht, The Netherlands). The µCT-based skull reconstructions were used for anatomical comparison and geometric morphometrics.

### Microscopy

Fluorescent images were acquired on a Zeiss Axio Observer.Z1 with an LSM 700 confocal microscope via ZEN 2010 software (version 6.0, Carl Zeiss MicroImaging, Oberkochen, Germany). Brightfield imaging of stained preparations was performed on a Leica MZ16F dissection microscope (Concord, ON, Canada) with a 12.8 megapixel digital camera (DP72, Olympus, Richmond Hill, ON, Canada). We selected lateral views captured of *sox10*:GFP positive fishes at 4 dpf for linear morphometrics (*n*=15 for wild-type; *n*=13 for *nkx3.2*$^{ua5011}$ zebrafish).

## Morphometrics

### Rationale for morphometric comparison

The purpose of this comparison was to quantitatively test the qualitative phenotypic similarities and differences among *nkx3.2*$^{-/-}$ mutants, wild-type zebrafish and anaspids (and thelodonts for gape angles). Within zebrafish, the skulls of *nkx3.2*$^{-/-}$ mutants morphologically depart from wild-type at adult stage (Fig. 2). To describe these morphological differences quantitatively, we compared skeletal growth between *nkx3.2*$^{-/-}$ and wild-type zebrafish. We also assessed similarities between the *nkx3.2*$^{-/-}$ phenotype and the general head configuration in anaspids and furcacaudiid thelodonts. Zebrafish and anaspids are phylogenetically distant: the former is a cypriniform nested deep within gnathostomes, whereas anaspids represent either a stem gnathostome or even a stem cyclostome lineage (Donoghue et al., 2000; Janvier, 2007; 1996; Keating and Donoghue, 2016; Miyashita et al., 2019). Furcacaudiids form a small group within thelodonts, a jawless stem gnathostome lineage (Märss et al., 2007; Wilson and Caldwell, 1993). The skull roof and facial bones of a zebrafish are macromeric. In contrast, the skull of an anaspid is largely micromeric with scales of acellular bone (Blom et al., 2001), and that of a thelodont also consists of micromeric scales with dentinous crowns and bases of acellular bone (Märss et al., 2007). There is no morphological correspondence in individual elements of the skull roof between zebrafish and anaspids. The parabranchial cavity is closed by the operculum in zebrafish, whereas each branchial pouch had its own outlet in the series of external pores in anaspids and thelodonts (Blom et al., 2001; Janvier, 1996). A single gene mutation in *nkx3.2* did not reverse these, and other morphological differences accumulated after the last common ancestor of zebrafish and anaspids. For morphometric comparison, we chose metric traits that could be identified in both zebrafish and anaspids.

### Linear morphometrics

We compared the gape among zebrafish, anaspids and thelodonts. In zebrafish, the angle was taken by extrapolating the axis of the premaxilla until it meets the axis of the dentary. At stages younger than the onset of dermal ossification (4 and 14 dpf), the angle was measured between the axes of the palatal process (palatoquadrate) and Meckel's cartilage. In anaspids, the upper and lower lips are demarcated by a series of plates or relatively larger scales, which allowed delineation of the gape angle (measured where the extrapolated upper and lower lip margins meet). The angle was measured similarly in thelodonts, except that the lip margins were identified along the series of small marginal scales. Gape angle exhibits a roughly normal distribution within each age class of both *nkx3.2*$^{-/-}$ and wild-type zebrafish and among anaspids (for original measurements, see Dryad data supplement 2, https://doi.org/10.5061/dryad.8w9ghx3j9). In addition to gape angles, we measured the length of the skull and lower jaw in zebrafish, and orbit diameter in anaspids and thelodonts.

### Geometric morphometics

Eight landmarks were assigned to both zebrafish (2 mpf) and anaspid samples for geometric morphometric comparison. These landmarks capture the general configuration of the head (1: anterior tip of upper lip; 2: junction between upper and lower lips; 3: anterior tip of lower lip; 4: nostril, or nasohypophyseal opening; 5: anterior extremity of orbit; 6: posterior extremity of orbit; 7: trunk–head boundary at dorsal outline; 8: ventral point of hypobranchial region). They describe structures that are homologous across vertebrates (landmarks 4, 5, 6) or geometrically determined comparable positions. They are free of morphological discontinuity between anaspids and gnathostomes (none of the landmarks represent anaspid- or gnathostome-specific morphology). TpsDig (Rohlf, 2018) was used to place landmarks on 2D images of anaspids and zebrafish. The digitized file was entered into MorphoJ software (Klingenberg, 2011) and all images were aligned using the anterior and posterior extremity of the orbits. These landmark data were transformed using the Procrustes superimposition method (Rohlf, 1999), and the resulting coordinates were compared using principal component analysis (PCA). In PCA, PC scores from anapsids, *nkx3.2*$^{+/+}$ and *nkx3.2*$^{-/-}$ zebrafish were grouped by equal frequency ellipses with a *P*-value of 0.95.

### Rationale for selection of comparative taxa in geometric morphometrics

From the pool of nearly a thousand cataloged specimens of anaspids, we selected a total of 70 specimens that show lateral compression during the fossilization process, with the least taphonomic distortion, to reflect the lateral view of the head. Furcacaudiid thelodonts were excluded from geometric morphometrics because only a handful of exceptionally preserved specimens are available; the sample size is small for this group (*n*<5), and all such specimens were collected from a single locality,

Journal of Experimental Biology (2020) 223, jeb216945. doi:10.1242/jeb.216945

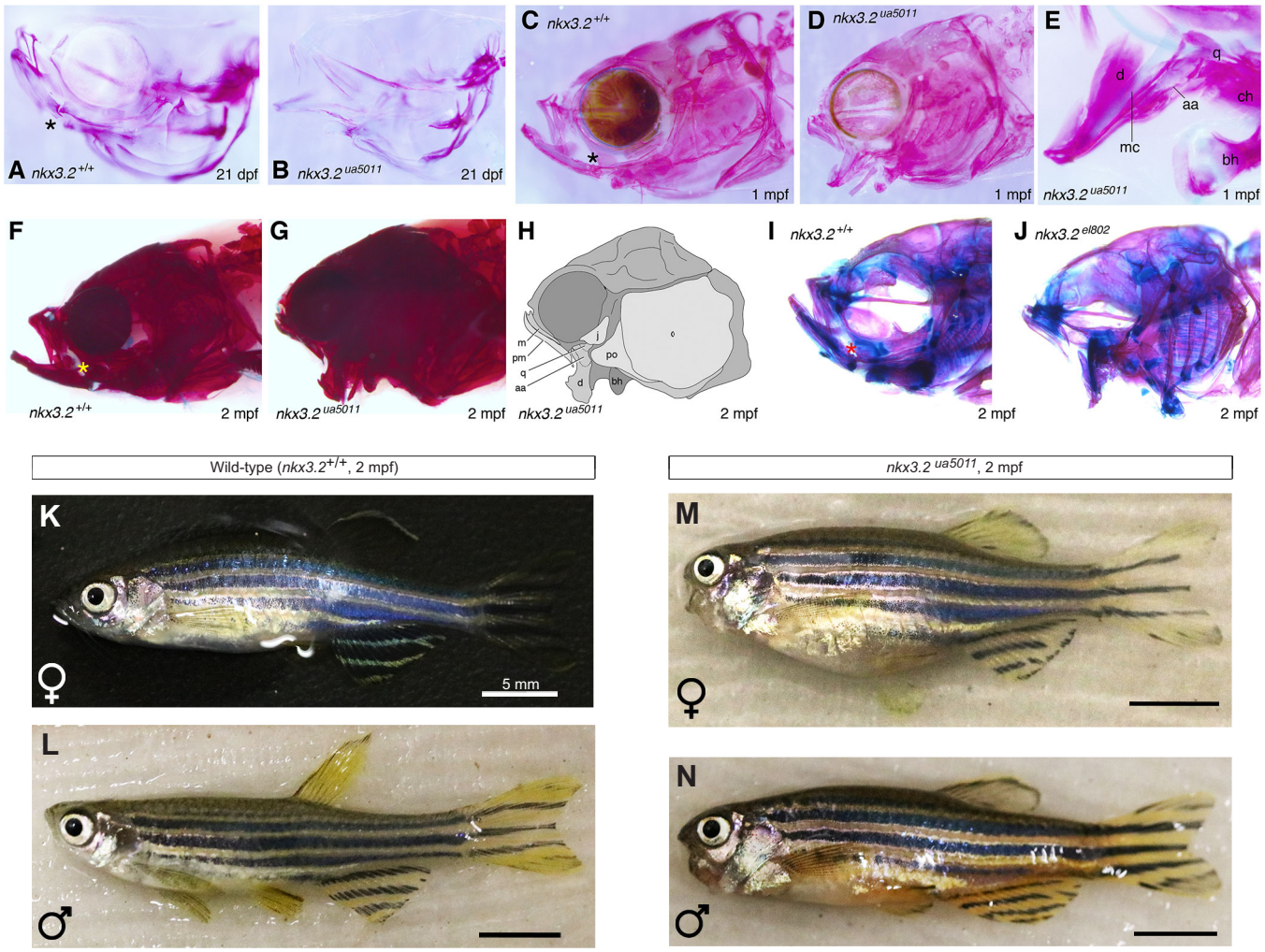


**Fig. 2. Ontogeny of *nkx3.2*$^{-/-}$ zebrafish documents drastic remodeling of the skull.** (A,B) Comparison of the skull morphology between age-matched wild-type (AB strain) (A) and *nkx3.2* homozygous mutant (*nkx3.2*$^{ua5011}$) (B) zebrafish at 21 dpf in right lateral view (inverted for consistency with other panels), using Alcian Blue and Alizarin Red staining. (C,D) Comparison of skull morphology between age-matched wild-type (C) and *nkx3.2*$^{ua5011}$ mutant (D) zebrafish at 1 month post-fertilization (mpf) in left lateral view, using Alcian Blue and Alizarin Red staining. (E) Detailed morphology of jaw skeleton in *nkx3.2*$^{ua5011}$ mutant at 1 mpf in right lateral view (inverted for consistency with other panels), using Alcian Blue and Alizarin Red staining. (F,G) Comparison of skull morphology between age-matched wild-type (F) and *nkx3.2*$^{ua5011}$ mutant (G) zebrafish at 2 mpf in left lateral view, using Alcian Blue and Alizarin Red staining. (H) Interpretive drawing of the specimen in G. (I,J) Comparison of skull morphology between age-matched wild-type (I) and *nkx3.2*$^{ua5011}$ mutant (J) zebrafish at 2 mpf in left lateral view, using Alcian Blue and Alizarin Red staining. This second independent null allele of *nkx3.2* confirms the phenotypes reported herein. (K–N) Comparison of overall morphology at 2 mpf among age-matched wild-type female (K) and male (L) and *nkx3.2*$^{el802}$ female (M) and male (N) zebrafish in left lateral view. Scale bars: 5 mm. For abbreviations, see Fig. 1.

making it difficult to identify (and thus control for) taphonomic artifacts. In addition, some landmarks could not be assigned confidently in this group. The transition from head to trunk is ambiguous because there is no apparent change in scale morphology (Wilson and Caldwell, 1993, 1998).

There are many other lineages of jawless vertebrates, including living cyclostomes, heterostracans, galeaspids and osteostracans (Janvier, 1996, 2007). Living cyclostomes are difficult to compare as they have an anguilliform profile and lack ossified skeletons, or cartilages unambiguously comparable to the jaw/lip elements of the zebrafish skull (Miyashita, 2012, 2016; Miyashita et al., 2019). Other jawless vertebrates generally have a depressiform profile (Janvier, 1996). For this reason, it is difficult to directly compare these agnathans with the compressiform zebrafish and anaspids. Some qualitative generalization is still possible. Furcacaudiid thelodonts have a lateromedially compressed body profile, and have a lip morphology consistent with that of anaspids (Wilson and Caldwell, 1998, 1993). These similarities suggest that depressed lower lips are a general condition in both cyclostome and gnathostome stems (Janvier, 1996), as reconstructed conventionally across these lineages.

## RESULTS

### Jaw joint is ankylosed in *nkx3.2* null alleles

At 4 dpf, *nkx3.2*$^{-/-}$ zebrafish replicated the *nkx3.2* morpholino knockdown phenotype: they lacked a jaw joint (Miller et al., 2003). The palatoquadrate and Meckel's cartilage fused together, and the retroarticular process was absent (Fig. 1D,G,I). Apart from joint ankylosis, no marked differences were apparent in overall

Journal of Experimental Biology (2020) 223, jeb216945. doi:10.1242/jeb.216945

morphology or survival rates between *nkx3.2*$^{-/-}$ mutants and wild-type at this stage (some minor differences in skull size and lower jaw proportions are discussed in the next section). Heterozygotes were morphologically indistinguishable from wild-type (Fig. 1C,F), and the *nkx3.2* alleles displayed recessive Mendelian inheritance ($F_2$ genotypes followed Mendelian ratio; heterozygotes developed wild-type morphology). Remarkably, these functionally jawless homozygous mutants survived beyond the early larval stages.

### Functionally jawless *nkx3.2*$^{-/-}$ zebrafish modify skull shape late in ontogeny

Despite the maladaptive nature of jaw dysfunctions in general, *nkx3.2*$^{-/-}$ zebrafish continued to grow without a jaw joint. Marked phenotypic differences from wild-type began to emerge between the 2nd and 3rd weeks post-fertilization (Fig. 2). The lower jaw became downturned in *nkx3.2*$^{-/-}$ fish, resulting in a fixed open mouth, whereas both upper and lower jaws were upturned in wild-type zebrafish (Fig. 2A,B). This timing coincides with the onset of ossification and the period of active feeding in normal juveniles (Cubbage and Mabee, 1996; Kimmel et al., 1995). Although the palatoquadrate and Meckel's cartilage remained fused in *nkx3.2*$^{-/-}$ mutants, skeletal staining revealed that the upper and lower jaw elements ossified independently of each other – still without a ball-and-socket joint structure (Fig. 3A,B). All skull elements in *nkx3.2*$^{-/-}$ mutants ossified without apparent delay.

The lower jaws were increasingly turned downward in *nkx3.2*$^{-/-}$ by the end of the first month, resulting in a greater gape (Fig. 2D,E). The jaw joint was still absent in *nkx3.2*$^{-/-}$ mutants: a sheet of perichondrium lay between the ossifying quadrate and articular – so the two bones remained distinct elements – but this interface had no other essential components of synovial diarthrosis (Fig. 3D,E). Many additional osteological differences emerged by this stage. Normally, the premaxilla and the maxilla swing forward to sit nearly vertical (Hernandez, 2000; Hernandez et al., 2007) (Fig. 2C). In *nkx3.2*$^{-/-}$ mutants, however, the premaxilla and the maxilla became oriented posteroventrally and abutted against the antorbital wall (Fig. 2D). The downturned lower jaws of the *nkx3.2*$^{-/-}$ mutants were relatively shorter than the normal lower jaws of wild-types. The basihyal protruded anteroventrally as much as the lower jaw, implying that the muscle connecting those two elements (m. intermandibularis posterior) (Schilling and Kimmel, 1997) may be responsible for lower jaw orientation. As a result of these modifications, *nkx3.2*$^{-/-}$ mutants had a shorter snout, a fixed open gape, and a dorsoventrally tall profile.

Linear morphometrics corroborated the departure from normal morphology in *nkx3.2*$^{-/-}$ mutants in the second half of the first month (14 dpf onward). For absolute size, no significant difference ($P$>0.05) in skull length emerged between wild-types and *nkx3.2*$^{-/-}$ mutants except at 4 dpf ($t$=2.202; $P$=0.338) (Fig. 4B). Also at this stage, the lower jaws appeared to be shorter relative to skull length in the mutants than in the wild-types ($t$=2.809; $P$=0.0078) (Fig. 4C). These minor but statistically significant differences at 4 dpf may have been due primarily to the fusion of jaw cartilages. By the second week, however, differences between the mutants and wild-types became non-significant in these metric traits. The lower jaw depression (gape angle >45 deg) in the mutants was pronounced at 21 dpf ($t$=−11.834; $P$<<0.01) (Fig. 4A), but proportional changes to lower jaw lengths in the same mutants were only expressed in significant magnitude at 1 month (21 dpf: $t$=1.7225; $P$=0.091559; 30 dpf: $t$=10.56; $P$<<0.01) (Fig. 4C). This lag indicates that the rate of skeletal growth shifted in the jaws after their orientations changed. Morphological variations within a cohort of *nkx3.2*$^{-/-}$ mutants were greater at this stage than in any other (Fig. 4A,C).

### Adult *nkx3.2*$^{-/-}$ skeletal morphology markedly departs from wild-type

At 2 months of age and approaching sexual maturity, nearly all *nkx3.2*$^{-/-}$ mutants had a gape angle greater than 90 deg (Fig. 4A).

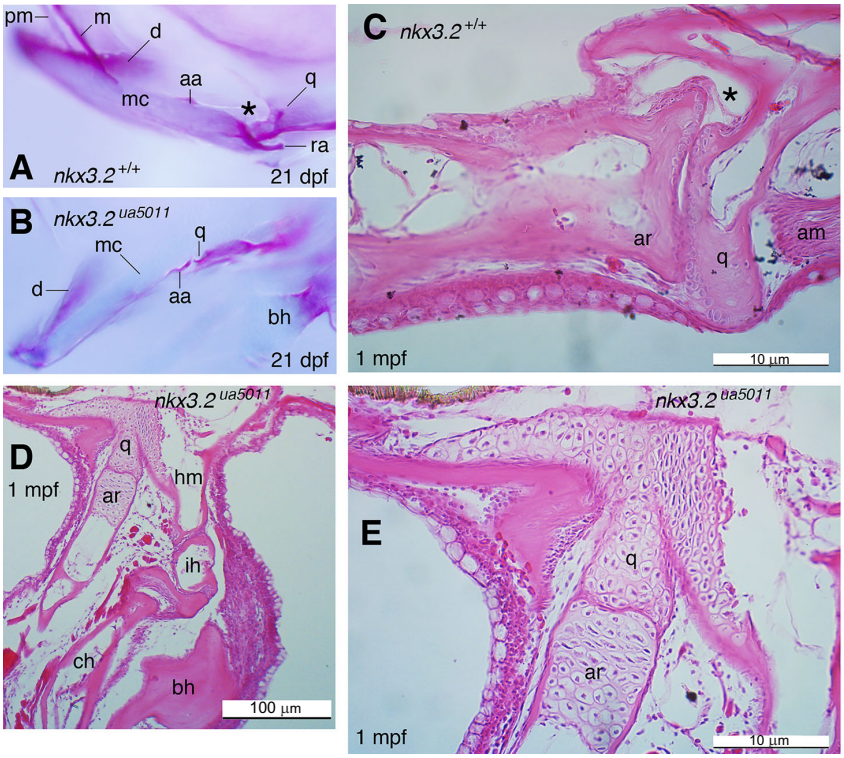


**Fig. 3. Detailed morphology of jaw joint in wild-type zebrafish, or the joint-less interface between the upper and lower jaws in *nkx3.2*$^{-/-}$ mutants.** (A,B) Detailed morphology of junction between the upper and lower jaws in age-matched wild-type (A) and *nkx3.2* homozygous mutant (*nkx3.2*$^{ua5011}$) (B) zebrafish at 21 dpf in left lateral view, using Alcian Blue and Alizarin Red staining. (C,D) Sagittal section of junction between the upper and lower jaws in age-matched wild-type (AB) (C) and *nkx3.2* homozygous mutant (*nkx3.2*$^{ua5011}$) (D) zebrafish at 1 mpf, stained with eosin and hematoxylin. (E) Detailed view of a section in D. For abbreviations, see Fig. 1.

Journal of Experimental Biology (2020) 223, jeb216945. doi:10.1242/jeb.216945

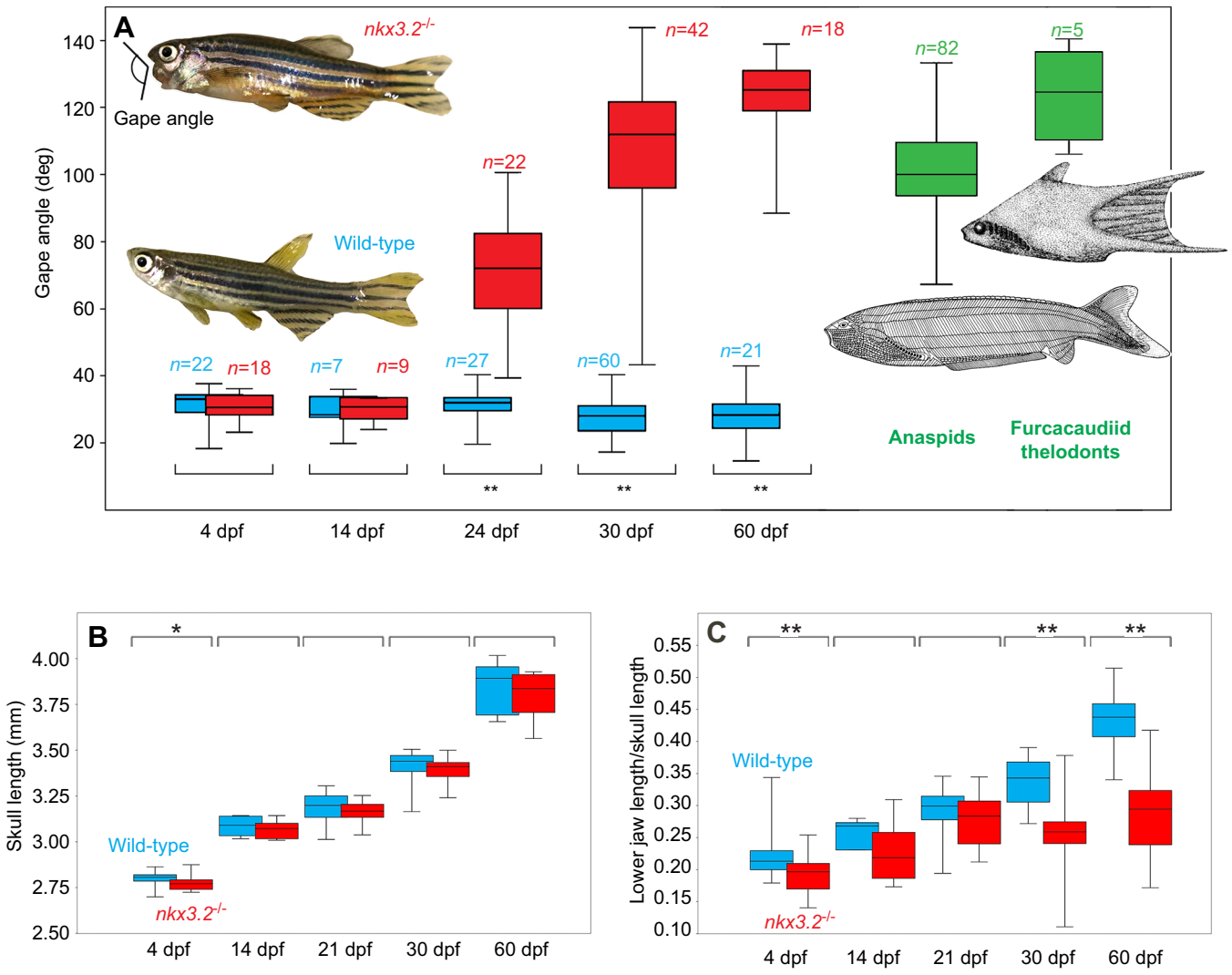


**Fig. 4. Growth of *nkx3.2*$^{-/-}$ mutants in linear and proportional traits.** (A) Ontogeny of gape angles in wild-type and mutant zebrafish. A marked departure from wild-type morphology (blue) occurs in lower jaw orientations of *nkx3.2*$^{-/-}$ zebrafish (red) past 14 dpf, coinciding in timing with metamorphosis (onset of ossification in the skulls and active suction feeding). Fixed open gapes in the mutants at 1–2 mpf are comparable to those of Paleozoic agnathan lineages, birkeniiform anaspids and furcacaudiid thelodonts (green). The orientations were measured here as gape, an angle between the upper and lower lips at a natural, resting position. (B) Overall skull growth in wild-type and mutant zebrafish. Wild-type and *nkx3.2*$^{-/-}$ zebrafish do not differ significantly from each other in absolute size, except at 4 dpf. Here, skull length is selected to illustrate this general observation. (C) Ontogeny of lower jaws in wild-type and mutant zebrafish. Proportional changes appear to follow shape changes in skeletal remodeling. The box plot shows phenotypic separation in relative lower jaw length between wild-type and *nkx3.2*$^{-/-}$ zebrafish at 1 and 2 mpf, even though a significant difference developed in lower jaw orientation by 21 dpf. Values are plotted as boxes of first and third quartile, with middle line displaying the mean, and whiskers indicating maximum and minimum values (*n*=sample size, across A–C). Asterisk indicates level of statistically significant difference in means (*t*-test, two-tailed): **P*<0.05; ***P*<0.01. Photographs of zebrafish are male representative specimens at 60 dpf (Fig. 2L,N). Drawings are: *Pharyngolepis oblonga* as a general representative of anaspids (after Blom et al., 2001; Kiaer, 1924); and *Furcacauda fredholmae* as a general representative of furcacaudiid thelodonts (after Wilson and Caldwell, 1993). See Dryad data supplement 2 (https://doi.org/10.5061/dryad.8w9ghx3j9) for all original measurements.

These *nkx3.2*$^{-/-}$ adults continued to be characterized by the morphological differences identified at 1 mpf. The skulls appeared to be shorter, wider and more highly ossified in *nkx3.2*$^{-/-}$ mutants than in wild-types (Figs 2 and 5; Movie 1). The short profile of the mutant skulls was primarily due to reduced relative size of the snout. With the premaxilla and maxilla held rigid, the kinethmoid – a sesamoid that acts as a hinge between upper jaw and skull roof (k in Fig. 5A,C,D; Hernandez et al., 2007) – was absent in the fully ossified *nkx3.2*$^{-/-}$ adults. The nostrils sat between the eyes in the mutants, whereas they were level with the anterior margin of the orbit in wild-types [compare nasals (na) with respect to lateral ethmoids (le) in Fig. 5A–F]. The skull width was apparently greater in the mutants than in the wild-type zebrafish across the skull roof and between the opercula (Fig. 5C–J). The circumorbital bones including supraorbital (sr) and jugal (j) became massive and flared laterally in the mutants (Fig. 5B). In comparison to wild-type zebrafish, the *nkx3.2*$^{-/-}$ mutants developed substantially larger basihyals (bh), laterally oriented ceratobranchials (cb), and a larger mass of bones and cartilages around the interface of the quadrate (q) and the articular (aa) (Fig. 5B,F,I,J). The occiput had a larger surface area for the epaxial muscles to attach to (Fig. 5B). All homozygous mutants showed the descriptive skeletal traits identified here. Morphologically, the

Journal of Experimental Biology (2020) 223, jeb216945. doi:10.1242/jeb.216945

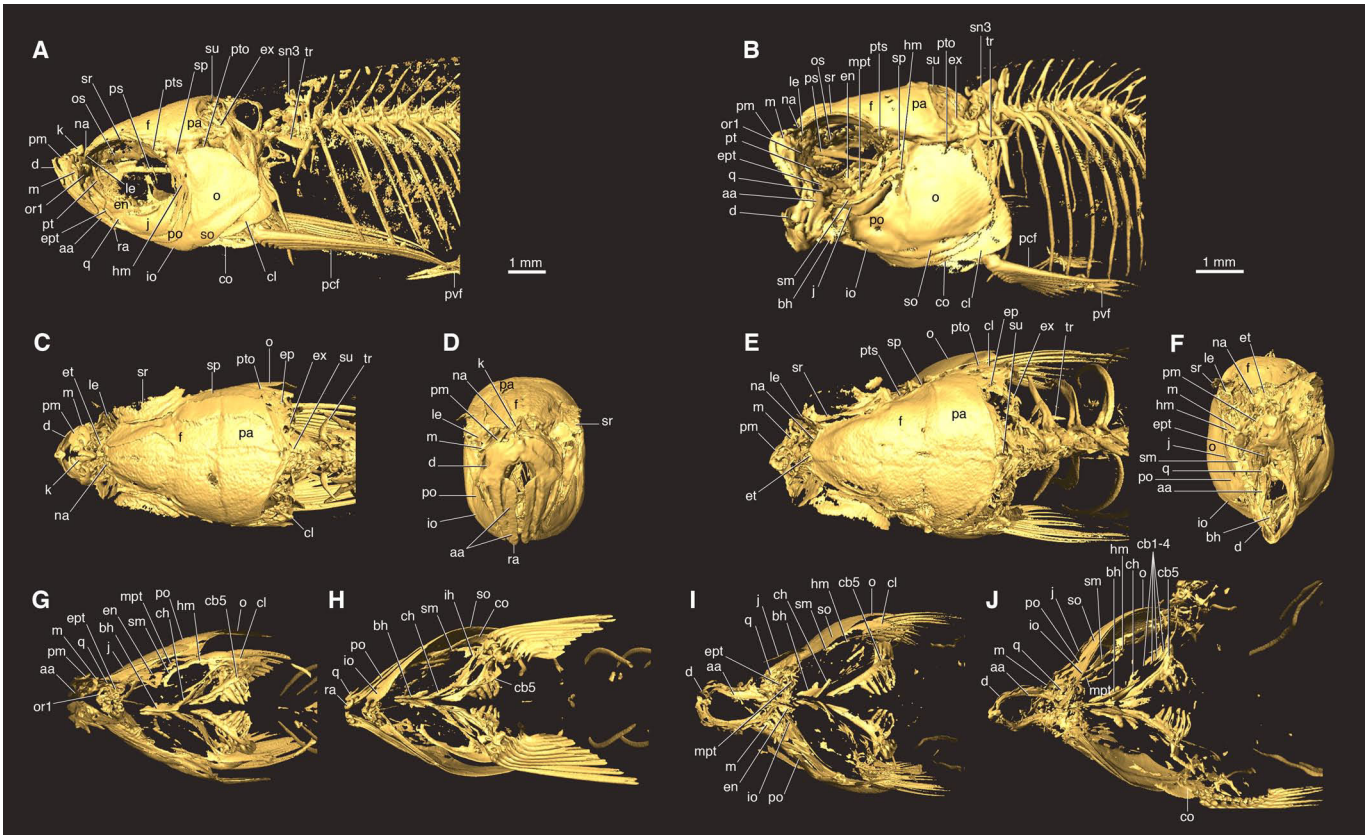


**Fig. 5. Micro-computed tomography (µCT)-based skeletal reconstructions of the adult wild-type and *nkx3.2*$^{-/-}$ mutant zebrafish.** Left: wild-type zebrafish (2 mpf, female) in (A) left lateral, (C) dorsal, (D) anterior, (G) anterodorsal, and (H) posteroventral views. Right: *nkx3.2* homozygous mutant (*nkx3.2*$^{ua5011}$) (2 mpf, female) zebrafish in (B) left lateral, (E) dorsal, (F) anterior, (I) anterodorsal and (J) posteroventral views. G–J show the skull interior with the neurocranium and skull roof virtually removed. The adult mutant displays dramatic phenotypes in the jaw, snout, lips and orobranchial regions. For abbreviations, see Fig. 1.

phenotypic effects of the two alleles (*nkx3.2*$^{ua5011}$ and *nkx3.2*$^{el802}$) were virtually indistinguishable from each other at respective ages (Fig. 2G,J), given variations within a strain (for examples, see variation in gape angle, relative length of lower jaws, or sexual dimorphism in *nkx3.2*$^{ua5011}$: Figs 2M,N and 4A,C).

### Adult *nkx3.2*$^{-/-}$ zebrafish alter feeding

With their modified skulls, adult *nkx3.2*$^{-/-}$ mutants exhibited feeding markedly different from wild-type. Wild-type zebrafish fed by suction in a sequence consistent with general teleost feeding mechanics (Alexander, 1969, 1970; Lauder, 1979, 1980; Westneat, 2004, 2005): rapid lower jaw depression; a forward swing of the mobile premaxilla–maxilla complex and head elevation; maximum expansion of the parabranchial cavity; and closing of the operculum, while holding themselves steady with backstrokes of the pectoral fins (Fig. 6A; Movie 1). In contrast, adult *nkx3.2*$^{-/-}$ mutants were constrained by the fixed upper jaw unit and open gape. They instead showed ram feeding (swimming through food) (Fig. 6B; Movie 1). The jaws remained fixed, and no significant movement was observed in the lips. The mutants elevated the head and the basihyal before ingesting food, shortly followed by maximum expansion of the parabranchial cavity (Fig. 6B). These externally visible movements may provide weak suction to assist the ram feeding. Whereas in wild-type one complete cycle of the jaw opening and closing took approximately 80 ms (and approximately one-tenth of a second to close the operculum), *nkx3.2*$^{-/-}$ mutants required double that time from changing direction of swimming toward the food (0 s) to doing so again away from the food (0.2 s) in the particular feeding episode in Fig. 6B.

This ram feeding was correlated with skull remodeling in *nkx3.2*$^{-/-}$ mutants. Until passing 1 mpf, the fusion between jaw cartilages was not completely ossified in these mutants, potentially allowing plastic deformation (Fig. 2E,L). These observations suggest that phenotypic changes (open mouth and ram feeding) accommodate functional jawlessness in *nkx3.2*$^{-/-}$ zebrafish.

### *nkx3.2*$^{-/-}$ zebrafish converge onto agnathans in overall head shape

Through this dramatic transformation, *nkx3.2*$^{-/-}$ zebrafish assumed a head shape reminiscent of two lineages of extinct jawless vertebrates that also have laterally compressed body profiles: (a) birkeniiform anaspids (Fig. 7C), stem cyclostomes known mostly from the Silurian period (Blom et al., 2001; Miyashita et al., 2019); and (b) furcacaudiid thelodonts (Fig. 7D), much more elusive stem gnathostomes known from the Silurian and Devonian periods (Märss et al., 2007; Wilson and Caldwell, 1998). Qualitatively, the resemblance is particularly striking in functional and proportional features, including: fixed gape (depressed lower lips), shortened snout, interorbital position of the nostril, relatively large branchial region and massive occiput.

In linear morphometrics, the gape angle revealed that *nkx3.2*$^{-/-}$ mutants closely resemble the anaspid- and thelodont-like conditions late in ontogeny (Fig. 4A). The trait in *nkx3.2*$^{-/-}$ mutants departed from the wild-type condition after the onset of skull ossification and active feeding (14–21 dpf), and overlapped with the range occupied by anaspids and thelodonts in later stages (1 and 2 mpf). When the jaws were at rest, the gape angle in wild-type zebrafish was

Journal of Experimental Biology (2020) 223, jeb216945. doi:10.1242/jeb.216945

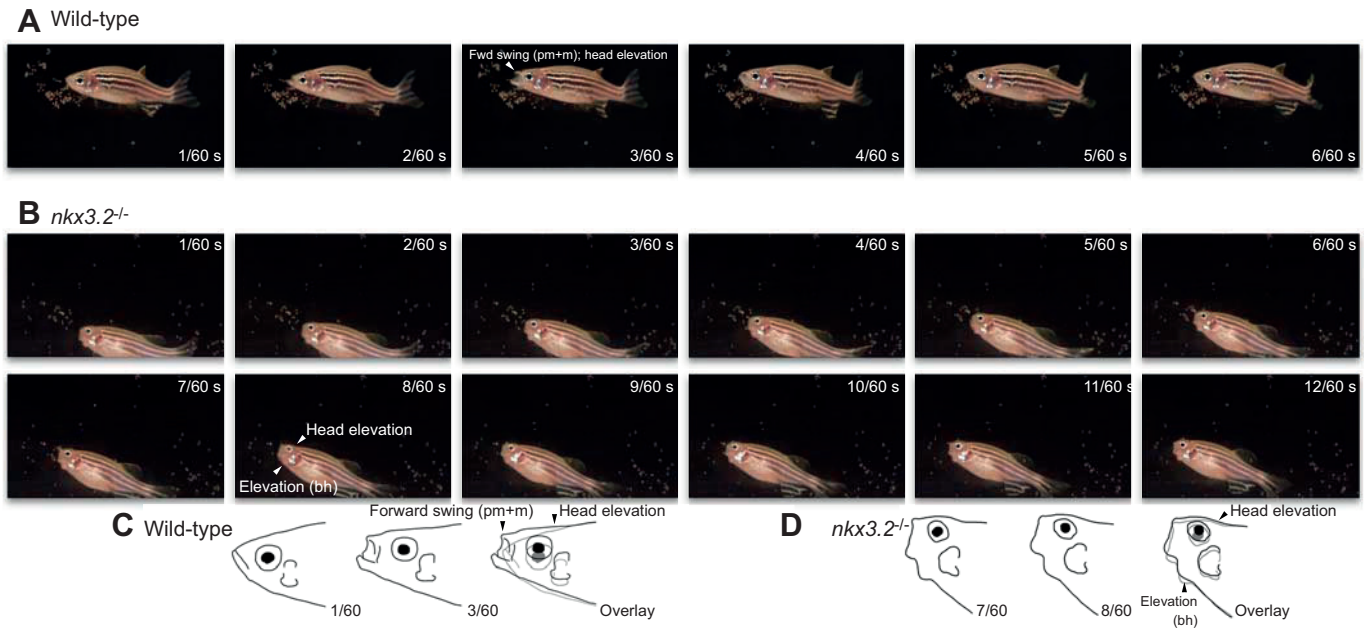


**Fig. 6. Functionally jawless *nkx3.2*$^{-/-}$ mutants perform ram feeding.** (A) Wild-type zebrafish (2 mpf) use suction feeding, following the general principles of suction feeding mechanics of actiopterygians: head elevation, lower jaw depression, forward swing of premaxilla and maxilla, maximum expansion of parabranchial cavity, and recoiling motions in that order. An entire cycle takes approximately 0.1 s. (B) No suction feeding was observed in *nkx3.2*$^{-/-}$ zebrafish (2 mpf); instead, they perform ram feeding (swim through food) with a fixed open gape. In this particular feeding episode, the mutant initiated a cycle with detection of food (change in swimming orientation) and turned laterally to exit that swimming trajectory in approximately 0.2 s. (C,D) Head outlines traced after individual frames of the wild-type and mutant feeding cycles (A,B) illustrating movements described for each genotype. Frame-by-frame still images from a film captured at 60 frames s$^{-1}$. See Movie 1.

consistently around 30 deg regardless of ontogenetic stage. This was also true for *nkx3.2*$^{-/-}$ mutants at 4 and 14 dpf when they still rely on yolk as the main or partial intake. The gape angle increased steadily thereafter in the mutants. In anaspids, the gape angle appeared to vary independently of body size. No correlation was detected between gape angle and orbit diameter in this clade ($r$=−0.114; $P$=0.306).

In landmark-based geometric morphometrics, *nkx3.2*$^{-/-}$ mutants aligned more closely with anaspids than wild-type zebrafish along the principal components (PCs) that explain the adult phenotype (PC1 and PC5) (Fig. 7E,F). Nearly one-third of the overall shape variation loaded on PC1 and primarily concerned anteroposterior length and dorsoventral height of the entire head. Compared with wild-type zebrafish, *nkx3.2*$^{-/-}$ mutants and most anaspids had a much shorter snout (with the lips and the nostrils shifting posteriorly toward the eye) and dorsoventrally deeper lower lips. PC 5 explained 7.0% of overall shape variation, and the traits that varied along it were orientation of lower lip and relative height of nostrils, which clearly set wild-type zebrafish apart from *nkx3.2*$^{-/-}$ mutants and anaspids. On the plot of PC1 and PC5, *nkx3.2*$^{-/-}$ mutants nearly entirely overlapped with anaspids in morphospace occupation and apart from wild-type zebrafish (Fig. 7F). PC2–4 (not shown in Fig. 7) largely explained variation among anaspids or within wild-type/mutant zebrafish samples and were therefore uninformative for comparison between the groups (see Dryad data supplement 3, https://doi.org/10.5061/dryad.8w9ghx3j9).

## DISCUSSION

### Mutants corroborate the function of *nkx3.2* in joint development

Our *nkx3.2*$^{-/-}$ zebrafish reinforce the morphant-based insight that this transcription factor is essential to the development of the jaw joint in non-mammalian vertebrates (Miller et al., 2003, 2004). This dependence is likely widespread among jawed vertebrates. *Nkx3.2* knockdown also results in fusion between the palatoquadrate and Meckel's cartilage in amphibians (Lukas and Olsson, 2018a), and a similar phenotype is observed in chicks with ectopic expression of BMP4 and FGF8 that repressed *Nkx3.2* (Wilson and Tucker, 2004). In mammals, the palatoquadrate (malleus) and Meckel's cartilage (incus) migrate to form middle ear ossicles. The malleus–incus joint is not affected in *Nkx3.2*$^{-/-}$ mice, but *Nkx3.2* plays a role in specification of the gonium and the anterior tympanic ring and maintains the malleus size (Tucker et al., 2004). Aside from its function in the head, *Nkx3.2* plays a role in various structures in mice and chicks, including the axial column (Herbrand et al., 2002; Lettice et al., 2001; Murtaugh et al., 2001) and visceral lateralities of the spleen and pancreas (Hecksher-Sørensen et al., 2004; Schneider et al., 1999). Comparing these phenotypes identified in amniote models with *nkx3.2*$^{-/-}$ zebrafish requires further analysis to determine the effect of *nkx3.2* loss of function on trunk morphology.

Thus, *nkx3.2* loss of function accounts for jaw joint ankylosis in the skulls of our mutant zebrafish. The bones forming the jaw joint develop from cartilages, and this corroborates previous findings about the regulatory role of Nkx3.2 in chondrogenesis. During development of the jaw joint, *nkx3.2* is thought to specify the joint interzone by inhibiting maturation or hypertrophy of the chondrocytes (Miller et al., 2003; Smeeton et al., 2016). Similar functions have been ascribed to *irx7* and *irx5a* in the hyoid joint (Askary et al., 2015). This is consistent with the predicted regulatory function of *Nkx3.2* in vertebral development, intervertebral and interphalangeal joint formation, or somatic chondrogenesis in general (Herbrand et al., 2002; Lettice et al., 2001; Murtaugh et al., 2001), via repression of *Runx2*, by upregulating *Col2α1* and/or through a positive feedback loop with *Sox9* (Smeeton et al., 2016). These

Journal of Experimental Biology (2020) 223, jeb216945. doi:10.1242/jeb.216945

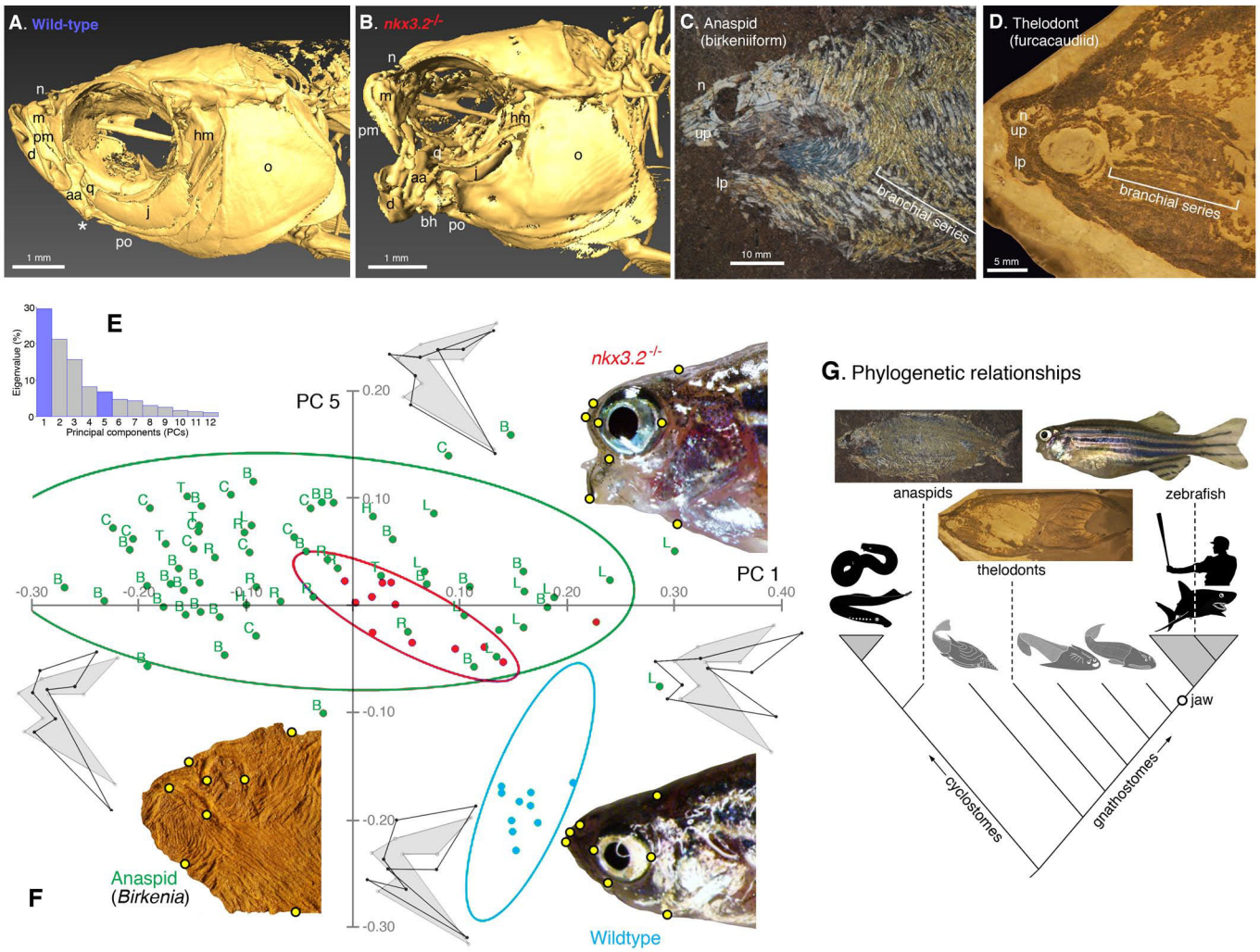


**Fig. 7. Adult *nkx3.2*$^{-/-}$ zebrafish converge onto overall head shapes of anaspids and thelodonts.** (A,B) Skulls of adult zebrafish in left lateral view via µCT imaging showing wild-type and *nkx3.2*$^{-/-}$ (Fig. 5A,B). The jaw joint is indicated by an asterisk in wild-type zebrafish (A) and is absent in mutant zebrafish (B). (C,D) Skulls of extinct jawless vertebrates, showing general resemblance to the skull shape of *nkx3.2*$^{-/-}$ zebrafish. (C) Skull of an anaspid (birkeniid birkeniiform) from the Upper Silurian Cape Philips Formation of Cornwallis Island, Canada (Geological Survey of Canada C-26661-005) in left lateral view. (D) Skull of *Sphenonectris turnerae*, a thelodont (furcacaudiid furcacaudiform) from the Lower Devonian Road River Formation of Northwest Territories, Canada (University of Alberta Laboratory for Vertebrate Palaeontology, specimen number 42212). For abbreviations, see Fig. 1. (E,F) Landmark-based geometric morphometric comparison of *nkx3.2* phenotype using the thin-plate-spline Procrustes superimposition and principal component (PC) analysis. (E) Histogram showing loadings on each principal component in eigenvalue (%). PC1 and PC5 are highlighted in blue. These two PCs were chosen for comparison between groups, as these are the two largest components that set *nkx3.2* homozygous mutants and wild-type zebrafish apart from each other at adult stage. (F) A Cartesian plot of PC1 and PC5, comparing morphospace occupation between wild-types (2 mpf) (blue), *nkx3.2* homozygous mutants (2 mpf) (red) and anaspids (green), each with 90% ellipse. The end of each axis is labeled with a thin-plate spline shape at that position (dark outline) against mean shape (gray silhouette). A representative specimen is shown with landmarks labeled (yellow circles) for each group in left lateral view. The anaspid example is *Birkenia elegans* (National Museum of Scotland specimen number 1929.5.6 from a Silurian locality of Scotland). Each data point is a unique biological replicate (a specimen). Anaspids are labeled with taxonomic identifications: B, *Birkenia elegans*; C, Birkeniidae indet. from the Cornwallis Island; H, *Pharyngolepis oblongus*; L, *Lasanius problematicus*; R, *Rycholepis parvulus*; T, *Pterygolepis nitidus*. See Dryad data supplement 1 (https://doi.org/10.5061/dryad.8w9ghx3j9) for original data. (G) Simplified phylogenetic tree of vertebrates to illustrate distant relationships among the taxa compared in this paper. A 60 dpf gravid female specimen is shown for *nkx3.2*$^{-/-}$ zebrafish (Fig. 3M). Photographs of an anaspid and a thelodont are the same individuals in the respective panels showing cranial morphology (C,D). Gray triangle indicates a crown group (not to scale). Dark silhouettes and long branches indicate crown groups, whereas gray silhouettes and short branches represent extinct lineages.

insights are based on: (a) experimental results using amniote embryos or somitic mesodermal cell cultures (Cairns et al., 2008; Kawato et al., 2012; Lengner et al., 2005; Murtaugh et al., 2001; Provot et al., 2006; Yamashita et al., 2009; Zeng et al., 2002); and (b) clinical and genetic studies of human pathologies, including osteoarthritis and spondylo-megaepiphyseal-metaphyseal dysplasia (including pseudoepiphyses) (Caron et al., 2015; Hellemans et al., 2009).

### Modifications to the skull follow the jaw joint loss

Although the fused jaw cartilages clearly result from *nkx3.2* mutation, *nkx3.2* loss of function, by itself, seems unlikely to yield the remaining phenotypic effects on skull form described here. Instead, the late onset and topology of changes to the skull morphology suggests that these modifications arose secondarily to jaw joint ankylosis. Other than fused jaw cartilages, *nkx3.2*$^{-/-}$

zebrafish appear normal until metamorphosis (14–21 dpf) (Fig. 1D,G). The open gape then becomes conspicuous, which likely began with m. intermandibularis posterior abducting the elastic Meckel's cartilage toward the basihyal.

As the skull ossifies, the observed phenotype becomes increasingly prominent (Fig. 2B,D,G,J,M,N). The skull bones arise endochondrally (quadrate, anguloarticular, basihyal) or intramembranously (premaxilla, maxilla, dentary, jugal, opercular, preopercular) (Cubbage and Mabee, 1996; Schilling and Kimmel, 1997). Much of the skeletal remodeling observed in adult *nkx3.2*$^{-/-}$ mutants occurred in the intramembranous bones, even though the known function of *nkx3.2* in skeletal development is exclusively related to cartilaginous structures (Chatterjee et al., 2011; Crotwell and Mabee, 2007; Miller et al., 2003; Smeeton et al., 2016). Except for the palatoquadrate and Meckel's cartilage, the highly modified endochondral skull bones in adult *nkx3.2*$^{-/-}$ mutants ossify spatially and temporarily well outside the known expression domain of *nkx3.2* (16 hpf to pre-metamorphosis; mandibular arch, sclerotomes and their derivatives, and midline fins) (Askary et al., 2017; Barske et al., 2018; Chatterjee et al., 2011; Crotwell and Mabee, 2007; Miller et al., 2003; Nair et al., 2007; Nichols et al., 2013).

Therefore, this dramatic modification of the skull comes second to the direct result of *nkx3.2* loss of function. To support this further, a genome-wide analysis suggests that *nkx3.2* patterning effects in the skull are restricted to the mid-portion of the mandibular arch (Askary et al., 2017). The hypertrophied mandibular cartilage (Fig. 5I) may result from *nkx3.2* loss of function in regulating local chondrogenesis (Smeeton et al., 2016). Still, further investigation is warranted for this hypertrophy, because in amphibians an ectopic cartilage formed in the mandibular arch with *Nkx3.2* overexpression, not repression (Lukas and Olsson, 2018b).

### Activities at jaw joint affect skull morphology

Functional jaw loss resulting from *nkx3.2* null mutations allowed the mutants to depart markedly in morphology from their wild-type cousins, despite the nearly identical genetic backgrounds. This departure implies that movements at the jaw joint can limit skull morphology. The specific combination of traits observed in adult *nkx3.2*$^{-/-}$ zebrafish – for example, nostrils in interorbital position, premaxilla and maxilla abutted against antorbital wall, basihyal protrusion – is likely maladaptive when the jaws function properly. In this regard, the absence of a kinethmoid in *nkx3.2*$^{-/-}$ mutants is a classic example. The sesamoid bone functions as a hinge in wild-type fish as the upper jaw swings forward against the skull roof (Hernandez et al., 2007). With the premaxilla and maxilla fixed in the mutants, however, the kinethmoid never formed as a distinct element (Fig. 5E). Our *nkx3.2*$^{-/-}$ zebrafish provide empirical evidence that jaw movements are an important factor in the development – and thus morphological diversity – of jawed vertebrate skulls.

Simultaneously, the absence of a jaw joint (or jaw apparatus altogether) also limits functionally viable forms. This interpretation is bolstered by the superficial convergence in head shapes between *nkx3.2*$^{-/-}$ zebrafish and two Paleozoic agnathan lineages (anaspids and furcacaudiform thelodonts). The *nkx3.2*$^{-/-}$ zebrafish and these agnathans share a functional condition – the absence of a hinge joint between upper and lower lips – and transversely compressed body profile. No evidence suggests any more similarities in the otherwise wild-type-like young mutants (Fig. 1D,G) until the lower jaw skeletons begin rotating posteroventrally after 14 dpf (Fig. 2B,D). Therefore, we interpret the anaspid/thelodont-like traits in the adult *nkx3.2*$^{-/-}$ zebrafish not as recapitulations of a conserved, genetically hard-wired ancestral development (atavism) but rather as parallel developmental responses to a shared functional constraint (convergence). This convergence implies that the vertebrate bauplan allows a limited repertoire of functionally viable morphological patterns in the skull.

A survey across vertebrates reveals many examples of jaw movements affecting bone morphology. Discrete variation in cichlid jaw morphology has an epigenetic basis in behaviorally mediated skeletal remodeling, where gaping frequencies in juveniles correlate with dimensions of the retroarticular process (Hu and Albertson, 2017). Additionally, dietary differences explain some taxonomically significant variations in the jaw morphology of multiple cichlid species (Galis, 1993; Greenwood, 1965; Liem and Osse, 1975; Meyer, 1987; Wimberger, 1992, 1991). Compared with cases in which jaw functions were perturbed, the magnitude of morphological changes in the adult *nkx3.2*$^{-/-}$ phenotype seems consistent with a series of surgical experiments in mammalian jaw skeletons (Bayram et al., 2010; Gomes et al., 2012; Horowitz and Shapiro, 1955; Lifshitz, 1976; Miyazaki et al., 2016; Rodrigues et al., 2009; Sarnat, 1970; Sarnat and Muchnic, 1971; Toledo et al., 2014) or with the 'bird face' deformity observed in clinical cases of the temporomandibular (=mammalian jaw) joint ankylosis in humans (El-Sheikh et al., 1996). Collectively, these studies imply a strong link between movements of the jaw skeletons and latent developmental potentials that shape the skulls.

### *nkx3.2*$^{-/-}$ zebrafish accommodate functional agnathia via plasticity

Jaw joint loss (*nkx3.2* loss-of-function phenotype) released *nkx3.2*$^{-/-}$ zebrafish from having to facilitate jaw movement, and exposed them to a different functional requirement: feeding without mobile jaws. The *nkx3.2*$^{-/-}$ mutants clearly altered their feeding. The mutants ram fed through the water column, whereas wild-type zebrafish typically maintained their position with pectoral backstrokes and used suction in a much faster feeding cycle (Fig. 6). Teleost fishes generally use head and basihyal elevation to assist suction (Westneat, 2004, 2005), but the *nkx3.2*$^{-/-}$ mutants retain these movements in a different functional context where there is no jaw motion. A fixed open gape accompanied by reduction of the snout is compatible with ram feeding and ventilating in the absence of the oral pump. The expanded branchial space facilitated by the greater skull width is also consistent with this. The massive occiput and basibranchial elements are likely linked to head elevation and basihyal retraction, respectively (Fig. 6B). At the onset of the open-mouth phenotype (2–3 weeks post-fertilization), cartilages are the main skeletal support of the jaws. The phenotypic effects become more pronounced as ossification proceeds around the deformed cartilaginous template (Fig. 2D). But all these correlated changes eventually lead to the well-constrained morphospace that *nkx3.2*$^{-/-}$ adults occupy (Fig. 7F). These results clearly point to developmentally plastic responses that coordinated changes in feeding and skull morphology and facilitated convergence with anaspids and thelodonts.

Remarkable convergence arises via developmental plasticity under similar functional requirements – even in the absence of homology in individual skeletal elements – between taxa widely separated chronologically and phylogenetically. Bichirs (*Polypterus*) routinely trained under terrestrial conditions develop modified pectoral fin skeletons, where induced, adaptive morphological changes parallel the traits observed among stem tetrapods (Standen et al., 2014). West-Eberhard (2005b) reviewed a goat born with congenital paralysis of the forelimbs, which performed bipedal locomotion. This behavioral

accommodation led to highly modified musculoskeletal anatomy of the axial column, pelvis and hindlimbs (Slijper, 1942a,b). Variation resulting from developmental plasticities – whether induced by environmental cues, developmental perturbation or mutation – are often non-random and adaptive (Palmer, 2012; West-Eberhard, 2003, 2005a,b). Therefore, as shown in *nkx3.2*$^{-/-}$ zebrafish, phenotypic accommodation of a defect resulting from a single null allele can initiate a set of correlated responses to form a complex trait independently acquired by a distant lineage, even after development has laid out lineage-specific patterns (such as homologies of individual bones).

Plasticity, whether at the level of whole-animal behavior or gene transcription, remains an elusive component of skeletal development that is challenging to test experimentally. Here, *nkx3.2*$^{-/-}$ zebrafish provide a unique experimental system. Many questions remain about these fish, including: what genetic mechanisms regulate the development of anomalous shapes of endochondral and intramembranous ossifications?; how are developmental pathways coordinated to respond to mechanical cues resulting from jaw joint dysfunction?; do mechanical interactions – especially those between developmentally independent, but functionally connected units such as the lower jaw and m. intermandibularis posterior – accurately predict morphological changes?; and finally, what is the cost of the *nkx3.2*$^{-/-}$ phenotype to fitness, and how does selection, in general, evaluate developmental plasticity?

## Developmental plasticity can explain phenocopies

The non-atavistic nature of the *nkx3.2*$^{-/-}$ phenotype potentially helps in re-evaluating evolutionarily inspired interpretations of phenocopies in developmental studies. There are no evolutionary relationships in the similarities between *nkx3.2*$^{-/-}$ zebrafish and anaspids or thelodonts. Anaspids are a stem cyclostome lineage (Miyashita et al., 2019) (Fig. 7G), and thus a poor surrogate for an ancestral state. The lineages between anaspids and thelodonts, or those between thelodonts and the gnathostome crown, do not share a similar combination of morphological traits, but instead are dorsoventrally depressed forms (Janvier, 1996; Miyashita, 2016; Miyashita et al., 2019). Finally, head similarities between the mutants and the stem taxa do not extend beyond overall configuration. No skull elements are lost or replaced in *nkx3.2*$^{-/-}$ zebrafish to achieve the anaspid/thelodont-like micromery (Blom et al., 2001; Janvier, 1996; Märss et al., 2007). Therefore, the adult *nkx3.2*$^{-/-}$ phenotype clearly does not represent a reversal to an ancestral state.

Experimental phenocopies (defective phenotypes resembling outgroup conditions) resulting from gene knockdowns and knockouts are often interpreted as atavistic (ancestral reversal), but alternative interpretations are seldom tested (Smith and Schneider, 1998). Epigenetic responses can correct or accommodate defective phenotypes resulting from perturbations to development (West-Eberhard, 2003). For example, normalization of craniofacial defects occurs via thyroid hormone-independent tissue remodeling in tadpoles of *Xenopus laevis* treated with *Sox6* morpholino, pharmacological inhibitors and ethanol (Pinet et al., 2019; Vandenberg et al., 2012). Here, our *nkx3.2*$^{-/-}$ zebrafish deployed a set of responses (modifications to the skull form and feeding) to accommodate a loss-of-function phenotype beyond correction (jaw joint ankylosis), while phenotypically resembling distant outgroups (anaspids and thelodonts) that lacked mobile jaws. Developmental plasticity is therefore a testable alternative to atavistic reversal to explain a phenocopy. By showing that a gnathostome can survive without a jaw, the anaspid/thelodont-like *nkx3.2*$^{-/-}$ zebrafish also offer a comparative model to make inferences about the functional morphology of these long-extinct agnathans.

### Acknowledgements

We thank B. F. Eames (University of Saskatchewan) for facilitating our collaboration; M. E. Bronner (California Institute of Technology), S. J. Childs (University of Calgary), M. I. Coates, R. K. Ho, V. E. Prince and M. W. Westneat (University of Chicago) for discussion; and members of the Allison and Prince labs for maintenance of the *nkx3.2*$^{ua5011}$ line.

### Competing interests

The authors declare no competing or financial interests.

### Author contributions

Conceptualization: T.M., J.S., A.R.P., J.G.C., W.A.; Methodology: T.M., P.B., J.S., A.P.O., W.A.; Formal analysis: T.M., P.B.; Investigation: T.M., P.B., J.S., A.P.O., N.N., B.G.; Resources: J.G.C., D.G., W.A.; Writing - original draft: T.M.; Writing - review & editing: T.M., P.B., J.S., A.R.P., D.G., W.A.; Visualization: T.M., P.B., J.S.; Supervision: A.R.P., J.G.C., D.G., W.A.; Project administration: W.A.; Funding acquisition: A.R.P., J.G.C., D.G., W.A.

### Funding

This work was supported by Natural Sciences and Engineering Research Council grants RGPIN-2014-04863, RGPIN-2014-06311 and RGPIN-2015-06006 (to A.R.P., D.G. and W.T.A., respectively) and National Institutes of Health grants R35DE027550 and K99 DE027218 (to J.G.C. and J.S., respectively). Deposited in PMC for release after 12 months.

### Data availability

Sequence information, measurements and landmark coordinates are available from the Dryad digital repository (Miyashita et al., 2020): https://doi.org/10.5061/dryad.8w9ghx3j9

### Supplementary information

Supplementary information available online at
https://jeb.biologists.org/lookup/doi/10.1242/jeb.216945.supplemental

### References

**Adekeye, E. O.** (1983). Ankylosis of the mandible: analysis of 76 cases. *J. Oral Maxillofac. Surg.* **41**, 442-449. doi:10.1016/0278-2391(83)90129-5

**Alexander, R. M.** (1969). Mechanics of the feeding action of a cyprinid fish. *J. Zool.* **159**, 1-15. doi:10.1111/j.1469-7998.1969.tb03067.x

**Alexander, R. M.** (1970). Mechanics of the feeding action of various teleost fishes. *J. Zool.* **162**, 145-156. doi:10.1111/j.1469-7998.1970.tb01261.x

**Askary, A., Mork, L., Paul, S., He, X., Izuhara, A. K., Gopalakrishnan, S., Ichida, J. K., McMahon, A. P., Dabizljevic, S., Dale, R. et al.** (2015). Iroquois proteins promote skeletal joint formation by maintaining chondrocytes in an immature state. *Dev. Cell* **35**, 358-365. doi:10.1016/j.devcel.2015.10.004

**Askary, A., Xu, P., Barske, L., Bay, M., Bump, P., Balczerski, B., Bonaguidi, M. A. Crump, J. G.** (2017). Genome-wide analysis of facial skeletal regionalization in zebrafish. *Development* **144**, 2994-3005. doi:10.1242/dev.151712

**Barske, L., Askary, A., Zuniga, E., Balczerski, B., Bump, P., Nichols, J. T. and Crump, J. G.** (2016). Competition between Jagged-Notch and Endothelin1 signaling selectively restricts cartilage formation in the zebrafish upper face. *PLoS Genet.* **12**, e1005967. doi:10.1371/journal.pgen.1005967

**Barske, L., Rataud, P., Behizad, K., Rio, L. D., Cox, S. G. and Crump, J. G.** (2018). Essential role of Nr2f nuclear receptors in patterning the vertebrate upper jaw. *Dev. Cell* **44**, 337-347.e5. doi:10.1016/j.devcel.2017.12.022

**Bayram, B., Uckan, S., Cetinsahin, A., Arman Ozcirpici, A., Ozdemir, H. and Yazici, C.** (2010). Repositioning of the masseter muscle and its effect on skeletal growth. *Oral Surg. Oral Med. Oral Pathol. Oral Radiol. Endodontol.* **109**, e1-e5. doi:10.1016/j.tripleo.2009.12.041

**Bixler, D., Ward, R. and Gale, D. D.** (1985). Agnathia-holoprosencephaly: A developmental field complex involving face and brain. Report of 3 cases. *J. Craniofac. Genet. Dev. Biol. Suppl.* **1**, 241-249.

**Blom, H., Märss, T. and Miller, C. G.** (2001). Silurian and earliest Devonian birkeniid anaspids from the Northern Hemisphere. *Earth Environ. Sci. Trans. R. Soc. Edinbur* **92**, 263-323. doi:10.1017/S0263593300000250

**Brown, D. M. and Marsh, J. L.** (1990). Agnathia and associated malformations: a case report. *Cleft Pal. J.* **27**, 415-418. doi:10.1597/1545-1569_1990_027_0415_aaamac_2.3.co_2

**Cairns, D. M., Sato, M. E., Lee, P. G., Lassar, A. B. and Zeng, L.** (2008). A gradient of Shh establishes mutually repressing somitic cell fates induced by Nkx3.2 and Pax3. *Dev. Biol.* **323**, 152-165. doi:10.1016/j.ydbio.2008.08.024

**Caron, M. M. J., Emans, P. J., Surtel, D. A. M., van der Kraan, P. M., van Rhijn, L. W. and Welting, T. J. M.** (2015). BAPX-1/NKX-3.2 acts as a chondrocyte hypertrophy molecular switch in osteoarthritis. *Arthritis Rheumatol.* **67**, 2944-2956. doi:10.1002/art.39293

**Cerny, R., Cattell, M., Sauka-Spengler, T., Bronner-Fraser, M., Yu, F. and Medeiros, D. M.** (2010). Evidence for the prepattern/cooption model of vertebrate jaw evolution. *Proc. Nat. Acad. Sci. USA* **107**, 17262-17267. doi:10.1073/pnas.1009304107

**Chatterjee, S., Bourque, G. and Lufkin, T.** (2011). Conserved and non-conserved enhancers direct tissue specific transcription in ancient germ layer specific developmental control genes. *BMC Dev. Biol.* **11**, 63. doi:10.1186/1471-213X-11-63

**Chidzonga, M. M.** (1999). Temporomandibular joint ankylosis: Review of thirty-two cases. *Brit. J. Oral. Maxillofac. Surg.* **37**, 123-126. doi:10.1054/bjom.1997.0089

**Crotwell, P. L. and Mabee, P. M.** (2007). Gene expression patterns underlying proximal–distal skeletal segmentation in late-stage zebrafish, *Danio rerio*. *Dev. Dyn.* **236**, 3111-3128. doi:10.1002/dvdy.21352

**Cubbage, C. C. and Mabee, P. M.** (1996). Development of the cranium and paired fins in the zebrafish *Danio rerio* (Ostariophysi, Cyprinidae). *J. Morphol.* **229**, 121-160. doi:10.1002/(SICI)1097-4687(199608)229:2<121::AID-JMOR1>3.0.CO;2-4

**Depew, M. J. and Simpson, C. A.** (2006). 21st Century neontology and the comparative development of the vertebrate skull. *Dev. Dyn.* **235**, 1256-1291. doi:10.1002/dvdy.20796

**Donoghue, P. C. J., Forey, P. L. and Aldridge, R. J.** (2000). Conodont affinity and chordate phylogeny. *Biol. Rev.* **75**, 191-251. doi:10.1017/S0006323199005472

**El-Sheikh, M. M., Medra, A. M. and Warda, M. H.** (1996). Bird face deformity secondary to bilateral temporomandibular joint ankylosis. *J. Cranio-Maxillofac. Surg.* **24**, 96-103. doi:10.1016/S1010-5182(96)80020-5

**Gagnon, J. A., Valen, E., Thyme, S. B., Huang, P., Ahkmetova, L., Pauli, A., Montague, T. G., Zimmerman, S., Richter, C. and Schier, A. F.** (2014). Efficient mutagenesis by Cas9 protein-mediated oligonucleotide insertion and large-scale assessment of single-guide RNAs. *PLoS ONE* **9**, e98186. doi:10.1371/journal.pone.0098186

**Galis, F.** (1993). Interactions between the pharyngeal jaw apparatus, feeding behaviour, and ontogeny in the cichlid fish, *Haplochromis piceatus*: a study of morphological constraints in evolutionary ecology. *J. Exp. Zool.* **267A**, 137-154. doi:10.1002/jez.1402670207

**Gekas, J., Li, B. and Kamnasaran, D.** (2010). Current perspectives on the etiology of agnathia-otocephaly. *Eur. J. Med. Genet.* **53**, 358-366. doi:10.1016/j.ejmg.2010.09.002

**Gillis, J. A., Modrell, M. S. and Baker, C. V. H.** (2013). Developmental evidence for serial homology of the vertebrate jaw and gill arch skeleton. *Nat. Commun* .**4**, 1436. doi:10.1038/ncomms2429

**Gomes, F. E. F., Moraes, R. B. and Luz, J. G. d. C.** (2012). Effects of temporal muscle detachment and coronoidotomy on facial growth in young rats. *Brazil. Oral. Res.* **26**, 348-354. doi:10.1590/S1806-83242012000400011

**Greenwood, P. H.** (1965). Environmental effects on the pharyngeal mill of a cichlid fish, *Astatoreochromis alluaudi*, and their taxonomic implications. *Proc. Linn. Soc. Lond* **176**, 1-10. doi:10.1111/j.1095-8312.1965.tb00932.x

**Hall, B. K.** (2015). *Bones and Cartilage: Developmental and Evolutionary Skeletal Biology*, 2nd edn London: Academic Press.

**Hecksher-Sørensen, J., Watson, R. P., Lettice, L. A., Serup, P., Eley, L., Angelis, C. D., Ahlgren, U. and Hill, R. E.** (2004). The splanchnic mesodermal plate directs spleen and pancreatic laterality, and is regulated by Bapx1/Nkx3.2. *Development* **131**, 4665-4675. doi:10.1242/dev.01364

**Hellemans, J., Simon, M., Dheedene, A., Alanay, Y., Mihci, E., Rifai, L., Sefiani, A., van Bever, Y., Meradji, M., Superti-Furga, A. et al.** (2009). Homozygous inactivating mutations in the NKX3-2 gene result in spondylo-megaepiphyseal-metaphyseal dysplasia. *Am. J. Hum. Genet.* **85**, 916-922. doi:10.1016/j.ajhg.2009.11.005

**Herbrand, H., Pabst, O., Hill, R. and Arnold, H.-H.** (2002). Transcription factors Nkx3.1 and Nkx3.2 (Bapx1) play an overlapping role in sclerotomal development of the mouse. *Mech. Dev.* **117**, 217-224. doi:10.1016/S0925-4773(02)00207-1

**Hernandez, L. P.** (2000). Intraspecific scaling of feeding mechanics in an ontogenetic series of zebrafish, *Danio rerio*. *J. Exp. Biol.* **203**, 3033-3043.

**Hernandez, L. P., Bird, N. C. and Staab, K. L.** (2007). Using zebrafish to investigate cypriniform evolutionary novelties: Functional development and evolutionary diversification of the kinethmoid. *J. Exp. Zool.* **308B**, 625-641. doi:10.1002/jez.b.21166

**Horowitz, S. L. and Shapiro, H. H.** (1955). Modification of skull and jaw architecture following removal of the masseter muscle in the rat. *Am. J. Phys. Anthropol.* **13**, 301-308. doi:10.1002/ajpa.1330130208

**Hu, Y. and Albertson, R. C.** (2017). Baby fish working out: an epigenetic source of adaptive variation in the cichlid jaw. *Proc. R. Soc. B* **284**, 20171018. doi:10.1098/rspb.2017.1018

**Janvier, P.** (2007). Homologies and evolutionary transitions in early vertebrate history. In *Major Transitions in Vertebrate Evolution* (ed. J. S. Anderson and H.-D. Sues), pp. 57-121. Bloomington: Indiana University Press.

**Janvier, P.** (1996). *Early Vertebrates, Oxford Monographs on Geology and Geophysics*. Oxford: Clarendon Press.

**Kawato, Y., Hirao, M., Ebina, K., Shi, K., Hashimoto, J., Honjo, Y., Yoshikawa, H. and Myoui, A.** (2012). Nkx3.2 promotes primary chondrogenic differentiation by upregulating Col2a1 transcription. *PLoS ONE* **7**, e34703. doi:10.1371/journal.pone.0034703

**Keating, J. N. and Donoghue, P. C. J.** (2016). Histology and affinity of anaspids, and the early evolution of the vertebrate dermal skeleton. *Proc. R. Soc. B* **283**, 20152917. doi:10.1098/rspb.2015.2917

**Kiaer, J.** (1924). The Downtonian fauna of Norway. I. Anaspida with a geological introduction. *Skrift* **6**, 1-139.

**Kimmel, C. B., Ballard, W. W., Kimmel, S. R., Ullmann, B. and Schilling, T. F.** (1995). Stages of embryonic development of the zebrafish. *Dev. Dyn.* **203**, 253-310. doi:10.1002/aja.1002030302

**Klingenberg, C. P.** (2011). MorphoJ: An integrated software package for geometric morphometrics. *Mol. Ecol. Resourc* **11**, 353-357. doi:10.1111/j.1755-0998.2010.02924.x

**Kuratani, S.** (2012). Evolution of the vertebrate jaw from developmental perspectives. *Evol. Dev.* **14**, 76-92. doi:10.1111/j.1525-142X.2011.00523.x

**Labun, K., Montague, T. G., Gagnon, J. A., Thyme, S. B. and Valen, E.** (2016). CHOPCHOP v2: A web tool for the next generation of CRISPR genome engineering. *Nuc. Acids Res.* **44**, W272-W276. doi:10.1093/nar/gkw398

**Lauder, G. V.** (1979). Feeding mechanics in primitive teleosts and in the halecomorph fish *Amia calva*. *J. Zool.* **187**, 543-578. doi:10.1111/j.1469-7998.1979.tb03386.x

**Lauder, G. V.** (1980). Evolution of the feeding mechanism in primitive actionopterygian fishes: a functional anatomical analysis of *Polypterus*, *Lepisosteus*, and *Amia*. *J. Morphol.* **163**, 283-317. doi:10.1002/jmor.1051630305

**Lengner, C. J., Hassan, M. Q., Serra, R. W., Lepper, C., van Wijnen, A. J., Stein, J. L., Lian, J. B. and Stein, G. S.** (2005). Nkx3.2-mediated repression of Runx2 promotes chondrogenic differentiation. *J. Biol. Chem.* **280**, 15872-15879. doi:10.1074/jbc.M411144200

**Lettice, L., Hecksher-Sørensen, J. and Hill, R.** (2001). The role of Bapx1 (Nkx3.2) in the development and evolution of the axial skeleton. *J. Anat.* **199**, 181-187. doi:10.1046/j.1469-7580.2001.19910181.x

**Liem, K. F. and Osse, J. W. M.** (1975). Biological versatility, evolution, and food resource exploitation in African cichlid fishes. *Integr. Comp. Biol.* **15**, 427-454. doi:10.1093/icb/15.2.427

**Lifshitz, J.** (1976). Comparative anatomic study of mandibular growth in rats after bilateral resections of superficial masseter, posterior temporal, and anterior digastric muscles. *J. Dent. Res.* **55**, 854-858. doi:10.1177/00220345760550052301

**Lukas, P. and Olsson, L.** (2018a). Bapx1 is required for jaw joint development in amphibians. *Evol. Dev.* **20**, 192-206. doi:10.1111/ede.12267

**Lukas, P. and Olsson, L.** (2018b). Bapx1 upregulation is associated with ectopic mandibular cartilage development in amphibians. *Zool. Lett.* **4**, 16. doi:10.1186/s40851-018-0101-3

**Manganello-Souza, L. C. and Mariani, P. B.** (2003). Temporomandibular joint ankylosis: Report of 14 cases. *International J. Oral. Maxillofac. Surg.* **32**, 24-29. doi:10.1054/ijom.2002.0308

**Märss, T., Turner, S. and Karatajūtė-Talimaa, V.** (2007). *Handbook of Paleoichthyology / "Agnatha" II. Thelodonti*. München: Verlag Dr. Friedrich Pfeil.

**Medeiros, D. M. and Crump, J. G.** (2012). New perspectives on pharyngeal dorsoventral patterning in development and evolution of the vertebrate jaw. *Dev. Biol.* **371**, 121-135. doi:10.1016/j.ydbio.2012.08.026

**Meyer, A.** (1987). Phenotypic plasticity and heterochrony in *Cichlasoma managuense* (Pisces, Cichlidae) and their implications for speciation in cichlid fishes. *Evolution* **41**, 1357-1369. doi:10.1111/j.1558-5646.1987.tb02473.x

**Miller, C. T., Yelon, D., Stainier, D. Y. R. and Kimmel, C. B.** (2003). Two endothelin 1 effectors, hand2 and bapx1, pattern ventral pharyngeal cartilage and the jaw joint. *Development* **130**, 1353-1365. doi:10.1242/dev.00339

**Miller, C. T., Maves, L. and Kimmel, C. B.** (2004). moz regulates Hox expression and pharyngeal segmental identity in zebrafish. *Development* **131**, 2443-2461. doi:10.1242/dev.01134

**Miyashita, T.** (2012). Comparative Analysis of the Anatomy of the Myxinoidea and the Ancestry of Early Vertebrate Lineages (*Unpublished M.Sc. thesis*). Edmonton: University of Alberta.

**Miyashita, T.** (2016). Fishing for jaws in early vertebrate evolution: a novel hypothesis of mandibular confinement. *Biol. Rev.* **91**, 611-657. doi:10.1111/brv.12187

**Miyashita, T., Coates, M. I., Farrar, R., Larson, P., Manning, P. L., Wogelius, R. A., Edwards, N. P., Anné, J., Bergmann, U., Palmer, A. R. et al.** (2019). Hagfish from the Cretaceous Tethys Sea and a reconciliation of the morphological–molecular conflict in early vertebrate phylogeny. *Proc. Nat. Acad. Sci. USA* **116**, 2146-2151. doi:10.1073/pnas.1814794116

**Miyashita, T., Baddam, P., Smeeton, J., Oel, A. P., Natarajan, N., Gordon, B., Palmer, A. R., Crump, G., Graf, D. and Allison, W. T.** (2020). nkx3.2 mutant zebrafish accommodate jaw joint loss through a phenocopy of the head shapes of Paleozoic jawless fish, v2, Dryad, Dataset, doi:10.5061/dryad.8w9ghx3j9

**Miyazaki, M., Yonemitsu, I., Takei, M., Kure-Hattori, I. and Ono, T.** (2016). The imbalance of masticatory muscle activity affects the asymmetric growth of

condylar cartilage and subchondral bone in rats. *Arc. Oral. Biol.* **63**, 22-31. doi:10.1016/j.archoralbio.2015.11.020

**Montague, T. G., Cruz, J. M., Gagnon, J. A., Church, G. M. and Valen, E.** (2014). CHOPCHOP: A CRISPR/Cas9 and TALEN web tool for genome editing. *Nuc. Acids Res.* **42**, W401-W407. doi:10.1093/nar/gku410

**Murtaugh, L. C., Zeng, L., Chyung, J. H. and Lassar, A. B.** (2001). The chick transcriptional repressor Nkx3.2 acts downstream of Shh to promote BMP-dependent axial chondrogenesis. *Dev. Cell* **1**, 411-422. doi:10.1016/S1534-5807(01)00039-9

**Nair, S., Li, W., Cornell, R. and Schilling, T. F.** (2007). Requirements for Endothelin type-A receptors and Endothelin-1 signaling in the facial ectoderm for the patterning of skeletogenic neural crest cells in zebrafish. *Development* **134**, 335-345. doi:10.1242/dev.02704

**Nichols, J. T., Pan, L., Moens, C. B. and Kimmel, C. B.** (2013). barx1 represses joints and promotes cartilage in the craniofacial skeleton. *Development* **140**, 2765-2775. doi:10.1242/dev.090639

**Palmer, A. R.** (2012). Developmental plasticity and the origin of novel forms: unveiling cryptic genetic variation via “use and disuse”. *J. Exp. Zool.* **318B**, 466-479. doi:10.1002/jez.b.21447

**Pinet, K., Deolankar, M., Leung, B. and McLaughlin, K. A.** (2019). Adaptive correction of craniofacial defects in pre-metamorphic *Xenopus laevis* tadpoles involves thyroid hormone-independent tissue remodeling. *Development* **146**, dev175893. doi:10.1242/dev.175893

**Provot, S., Kempf, H., Murtaugh, L. C., Chung, U., Kim, D.-W., Chyung, J., Kronenberg, H. M. and Lassar, A. B.** (2006). Nkx3.2/Bapx1 acts as a negative regulator of chondrocyte maturation. *Development* **133**, 651-662. doi:10.1242/dev.02258

**Rodrigues, L., Traina, A. A., Nakamai, L. F. and Luz, J. d. C.** (2009). Effects of the unilateral removal and dissection of the masseter muscle on the facial growth of young rats. *Brazil. Oral. Res.* **23**, 89-95. doi:10.1590/S1806-83242009000100015

**Rohlf, F. J.** (1999). Shape statistics: Procrustes superimpositions and tangent spaces. *J. Classific* **16**, 197-223. doi:10.1007/s003579900054

**Rohlf, F. J.** (2018). *tpsDIG*. New York.

**Sarnat, B. G.** (1970). The face and jaws after surgical experimentation with the septovomeral region in growing and adult rabbits. *Act. Oto-Laryngol.* **69**, 1-30. doi:10.3109/00016487009131762

**Sarnat, B. G. and Muchnic, H.** (1971). Facial skeletal changes after mandibular condylectomy in the adult monkey. *J. Anat.* **108**, 323-338. doi:10.1016/0002-9416(71)90180-1

**Schiffer, C., Tariverdian, G., Schiesser, M., Thomas, M. C. and Sergi, C.** (2002). Agnathia-otocephaly complex: report of three cases with involvement of two different Carnegie stages. *Am. J. Med. Genet.* **112**, 203-208. doi:10.1002/ajmg.10672

**Schilling, T. F. and Kimmel, C. B.** (1997). Musculoskeletal patterning in the pharyngeal segments of the zebrafish embryo. *Development* **124**, 2945-2960.

**Schneider, A., Mijalski, T., Schlange, T., Dai, W., Overbeek, P., Arnold, H.-H. and Brand, T.** (1999). The homeobox gene it NKX3.2 is a target of left–right signalling and is expressed on opposite sides in chick and mouse embryos. *Curr. Biol.* **9**, 911-9S1. doi:10.1016/S0960-9822(99)80397-2

**Slijper, E. J.** (1942a). Biologic-anatomical investigations on the bipedal gait and upright posture in mammals, with special reference to a little goat, born without forelegs. I. *Proc. Koninkl. Nederland. Akad. Wetenschap* **45**, 288-295.

**Slijper, E. J.** (1942b). Biologic-anatomical investigations on the bipedal gait and upright posture in mammals, with special reference to a little goat, born without forelegs. II. *Proc. Koninkl. Nederland. Akad. Wetenschap* **45**, 407-415.

**Smeeton, J., Askary, A. and Gage Crump, J.** (2016). Building and maintaining joints by exquisite local control of cell fate. *WIREs Dev. Biol.* **6**, e245. doi:10.1002/wdev.245

**Smith, K. K. and Schneider, R. A.** (1998). Have gene knockouts caused evolutionary reversals in the mammalian first arch? *BioEssays* **20**, 245-255. doi:10.1002/(SICI)1521-1878(199803)20:3<245::AID-BIES8>3.0.CO;2-Q

**Standen, E. M., Du, T. Y. and Larsson, H. C. E.** (2014). Developmental plasticity and the origin of tetrapods. *Nature* **513**, 54-58. doi:10.1038/nature13708

**Toledo, L. G., Cavalcanti, S. C. X. B., Corrêa, L. and Luz, J. G. C.** (2014). Effects of injury or removal of the articular disc on maxillomandibular growth in young rats. *J. Oral Maxillofac. Surg.* **72**, 2140-2147. doi:10.1016/j.joms.2014.06.445

**Tucker, A. S., Watson, R. P., Lettice, L. A., Yamada, G. and Hill, R. E.** (2004). Bapx1 regulates patterning in the middle ear: altered regulatory role in the transition from the proximal jaw during vertebrate evolution. *Development* **131**, 1235-1245. doi:10.1242/dev.01017

**Vandenberg, L. N., Adams, D. S. and Levin, M.** (2012). Normalized shape and location of perturbed craniofacial structures in the *Xenopus* tadpole reveal an innate ability to achieve correct morphology. *Dev. Dyn.* **241**, 863-878. doi:10.1002/dvdy.23770

**West-Eberhard, M. J.** (2003). *Developmental Plasticity and Evolution*, 1st ed. Oxford; New York: Oxford University Press.

**West-Eberhard, M. J.** (2005a). Developmental plasticity and the origin of species differences. *Proc. Nat. Acad. Sci. USA* **102**, 6543-6549. doi:10.1073/pnas.0501844102

**West-Eberhard, M. J.** (2005b). Phenotypic accommodation: adaptive innovation due to developmental plasticity. *J. Experimental Zool.* **304B**, 610-618. doi:10.1002/jez.b.21071

**Westneat, M. W.** (2004). Evolution of levers and linkages in the feeding mechanisms of fishes. *Integr. Comp. Biol.* **44**, 378-389. doi:10.1093/icb/44.5.378

**Westneat, M. W.** (2005). Skull biomechanics and suction feeding in fishes. *Fish Physiol. Fish Biomechanics*. **23**, 29-75. doi:10.1016/S1546-5098(05)23002-9

**Wilson, M. V. H. and Caldwell, M. W.** (1993). New Silurian and Devonian fork-tailed “thelodonts” are jawless vertebrates with stomachs and deep bodies. *Nature* **361**, 442-444. doi:10.1038/361442a0

**Wilson, M. V. H. and Caldwell, M. W.** (1998). The Furcacaudiformes: a new order of jawless vertebrates with thelodont scales, based on articulated Silurian and Devonian fossils from northern Canada. *J. Vert. Paleontol.* **18**, 10-29. doi:10.1080/02724634.1998.10011031

**Wilson, J. and Tucker, A. S.** (2004). Fgf and Bmp signals repress the expression of Bapx1 in the mandibular mesenchyme and control the position of the developing jaw joint. *Dev. Biol.* **266**, 138-150. doi:10.1016/j.ydbio.2003.10.012

**Wimberger, P. H.** (1991). Plasticity of jaw and skull morphology in the neotropical cichlids *Geophagus brasiliensis* and *G. steindachneri*. *Evolution* **45**, 1545-1563. doi:10.1111/j.1558-5646.1991.tb02662.x

**Wimberger, P. H.** (1992). Plasticity of fish body shape. The effects of diet, development, family and age in two species of *Geophagus* (Pisces: Cichlidae). *Biol. J. Linn. Soc.* **45**, 197-218. doi:10.1111/j.1095-8312.1992.tb00640.x

**Yamashita, S., Andoh, M., Ueno-Kudoh, H., Sato, T., Miyaki, S. and Asahara, H.** (2009). Sox9 directly promotes Bapx1 gene expression to repress Runx2 in chondrocytes. *Exp. Cell Res.* **315**, 2231-2240. doi:10.1016/j.yexcr.2009.03.008

**Zeng, L., Kempf, H., Murtaugh, L. C., Sato, M. E. and Lassar, A. B.** (2002). Shh establishes an Nkx3.2/Sox9 autoregulatory loop that is maintained by BMP signals to induce somitic chondrogenesis. *Genes Dev.* **16**, 1990-2005. doi:10.1101/gad.1008002